3 Biotech (2023) 13:174
https://doi.org/10.1007/s13205-023-03595-y

ORIGINAL ARTICLE

# Evaluation of therapeutic potentials of selected phytochemicals against Nipah virus, a multi-dimensional in silico study

**Deblina Rababi**[1] · **Anish Nag**[1]

Received: 11 February 2023 / Accepted: 26 April 2023 / Published online: 10 May 2023


## Abstract

The current study attempted to evaluate the potential of fifty-three (53) natural compounds as Nipah virus attachment glycoprotein (NiV G) inhibitors through in silico molecular docking study. Pharmacophore alignment of the four (4) selected compounds (Naringin, Mulberrofuran B, Rutin and Quercetin 3-galactoside) through Principal Component Analysis (PCA) revealed that common pharmacophores, namely four H bond acceptors, one H bond donor and two aromatic groups were responsible for the residual interaction with the target protein. Out of these four compounds, Naringin was found to have the highest inhibitory potential (−9.19 kcal $mol^{-1}$) against the target protein NiV G, when compared to the control drug, Ribavirin (−6.95 kcal $mol^{-1}$). The molecular dynamic simulation revealed that Naringin could make a stable complex with the target protein in the near-native physiological condition. Finally, MM-PBSA (Molecular Mechanics-Poisson–Boltzmann Solvent-Accessible Surface Area) analysis in agreement with our molecular docking result, showed that Naringin (−218.664 kJ $mol^{-1}$) could strongly bind with the target protein NiV G than the control drug Ribavirin (−83.812 kJ $mol^{-1}$).

**Keywords** Nipah virus · Phytochemicals · Drug-likeliness · In silico · Molecular docking · Statistics · Simulation

## Introduction

In the recent past, the world witnessed the COVID-19 pandemic caused by SARS-CoV-2 (Hu et al. 2021). Nipah virus (NiV), a deadly emergent infectious agent which has the potential to give rise to the next pandemic, causes severe respiratory illness and fatal encephalitis (Ahmad 2014; Thakur et al. 2022). Research is difficult to do on the live virus as it is a biosafety level 4 pathogen (BSL-4) (Tigabu et al. 2014). It belongs to the genus *Henipavirus* of the order *Mononegavirales*, family *Paramyxoviridae*, and subfamily *Paramyxovirinae* (Chua et al. 2000). The virus was named after Kampung Sungai Nipah village in Malaysia, first detected in 1998 (Chattu et al. 2018). The fruit-eating bats of *Pteropus* spp. are the primary reservoirs of the virus (Chua et al. 2002). This zoonotic agent transmits from infected animals to humans and, in turn, from one infected human to the other, mainly through respiratory droplets, body fluids, blood and urine (Gurley et al. 2007; de Wit and Munster 2015). So far, 639 human cases of Nipah virus infection have been reported from Malaysia, Bangladesh, the Philippines, Singapore and India (Devnath and Masud 2021). Despite being short-lived, the past outbreaks of the Nipah virus claimed many human lives and were associated with high mortality rates (40–75%) (Vanitha et al. 2019). In its 2018 research and development blueprint, the World Health Organisation (WHO) stressed the gravity of the threat to humanity and called for immediate attention regarding effective drug development (Mehand et al. 2018). Nipah is an enveloped virus with a negative-sense single-stranded RNA. The non-segmented viral genome codes for several structural and non-structural proteins and is about 18.2 kb in size. The analysis of the viral genome demonstrates an arrangement of six genes, namely nucleocapsid (N), phosphoprotein (P), matrix (M), fusion glycoprotein (F), attachment glycoprotein (G) and long polymerase (L). The P gene encodes P protein and three important accessory proteins, C, W and V (Martinez-Gil et al. 2017). Among all the proteins of Nipah, the attachment glycoprotein, NiV G plays a vital role in attachment with the host receptor, Ephrin B2 or B3. This protein primarily drives the spread of the infection by cell-to-cell fusion. Therefore, the interruption of viral entry into the cell can be brought about by blocking the active

✉ Anish Nag
anish.nag@christuniversity.in

[1] Department of Life Sciences, Bangalore Central Campus, CHRIST (Deemed to be University), Bangalore, India

site of NiV G responsible for host receptor interaction. This makes NiV G an attractive target for identifying potential anti-Nipah drugs, as currently, there are no approved therapeutics for Nipah virus infection (Geisbert et al. 2021). The treatment of infected patients is limited to supportive care (Ang et al. 2018).

Nevertheless, antiviral medications such as Ribavirin and Acyclovir were used to treat Nipah infection during past outbreaks in Malaysia and Singapore. However, they were not fully effective in curing Nipah-infected individuals (Sharma et al. 2019). The vaccines being developed by scientists worldwide are yet to be time-tested to validate their effectiveness against the infection. Initial deployment of bioinformatics tools for the preliminary screening of drugs may reduce the cost and improve the turnover time significantly. Many drug candidates can be screened quickly, efficiently and cost-effectively using a bioinformatics approach like computer-aided drug design (CADD) (Gaieb et al. 2019). A few in silico studies showed the potential of small molecules against the target proteins of the Nipah virus. However, these studies were not backed by statistical analysis (Ropón-Palacios et al. 2020; Kalbhor et al. 2021; Glaab et al. 2021).

Phytochemicals have long been used to develop novel drugs and identify potential drug candidates against emerging infectious diseases considering their efficacy and safety compared with their synthetic counterparts. Anaemia, jaundice, and teratogenic effects are some side effects of Ribavirin (Chong et al. 2001). The side effects of Acyclovir are nausea, vomiting and headaches (Miserocchi et al. 2007). Plant-derived compounds are known for their usage as medicines traditionally (Nandagoapalan et al. 2016). Phytochemical classes such as flavonoids, terpenoids, phenols, xanthophylls, carotenoids, and essential oils are known for their immunomodulatory, antitumor, antimicrobial, and antioxidant properties. These compounds have successfully entered the modern world of drug development, one of the reasons being their prominent antiviral activities (Byler et al. 2016; Ben-Shabat et al. 2020; Pandey et al. 2021). We previously published a few research articles on the role of phytochemicals against viral targets using in silico strategy. Curcumin, for example, identified in our *in-silico* study, was later found to be effective against the SARS-CoV-2 variant in a clinical study (Pawar et al. 2021; Nag et al. 2021b, 2022a). This presents the scope for extending this approach to identify anti-Nipah compounds. Identification of phytocompounds as potential anti-Nipah drug candidates requires evaluation of the chemistry and stability of their binding interaction with Nipah proteins which can be facilitated through the integration of molecular docking study, molecular alignment of ligands (pharmacophore) and analysis of molecular dynamic simulation.

In this work, fifty-three (53) phytochemicals and the control drug, Ribavirin were tested for Nipah G protein inhibition potential through an in silico molecular docking study. Further, drug-like properties of the selected phytochemicals were also evaluated. We combined statistical and pharmacophore approaches to identify functional descriptors responsible for protein–ligand interaction. Finally, the stability of the ligand–protein complex was studied using the molecular dynamic simulation technique.

## Materials and methodology

### Preparation of the protein

The three-dimensional structure of the Nipah virus attachment glycoprotein (NiV G) in complex with the human cell receptor, Ephrin B2 (PDB id 2VSM, Chain A and B, X-Ray Diffraction, Resolution 1.8 Å) was downloaded from the RCSB PDB (https://www.rcsb.org/). This selection was based on the high resolution of the crystal structure (1.8 Å), determined by the X-ray diffraction methodology (Berman et al. 2002). Nipah virus attachment glycoprotein chain A (NiV G:A) was selected as the target protein for this study by using UCSF Chimera software (Pettersen et al. 2004). The heteroatoms and water molecules in the receptor protein were removed using Discovery Studio 2021 (Makhloufi et al. 2022). Maestro 13.3 and SwissPDB viewer were used for editing the protein structure, including removing non-polar hydrogens and adding polar hydrogens to the receptor protein and energy minimization at the physiological (pH 7.4) (Trott and Olson 2009). Additionally, the three-dimensional structure of the human cell receptor, Ephrin B2 (NiV G:B) was optimised for molecular docking using a similar methodology followed for Nipah virus attachment glycoprotein chain A.

### Preparation of ligands

Fifty-three (53) phytochemicals, along with control drugs Ribavirin and Acyclovir were downloaded from the PubChem database (https://pubchem.ncbi.nlm.nih.gov/) and considered as ligands for this study (Kim et al. 2019). Ribavirin was commonly used as an antiviral agent in the literature. Tang et al. 2019 used Ribavirin as a control drug for inhibiting viral entry, in vivo. Further, in another study, it was found to inhibit Nipah virus glycoprotein in silico (Ghimire et al. 2022). Considering these evidences, Ribavirin was selected as the control drug for our work. Acyclovir was administered to workers in Singapore during Nipah virus outbreak in 1999. Hence, Acyclovir was also selected as a control drug in this study (Hauser et al. 2021). The three-dimensional structures of the phytochemicals were downloaded from PubChem in "SDF" format. The phytochemicals were structurally optimized

and converted to "PDB" format using Avogadro software. This step was followed as a prerequisite for conducting molecular docking studies. For optimization of the ligands, a universal force field (UFF) algorithm was applied for the energy minimization of the ligands, followed by adding polar hydrogens to the ligands at pH, 7.4 (Hanwell et al. 2012; Nag et al. 2021b, 2023; Cho et al. 2022). Two-dimensional structures of the ligands are represented in Fig. 1.

## Active site prediction and molecular docking

### Protein–protein docking

The protein–protein docking studies for Nipah virus attachment glycoprotein (NiV G) in complex with the human cell receptor, Ephrin B2 were performed using ClusPro 2.0 docking server (https://cluspro.bu.edu/login.php) (Kozakov et al. 2017). PIPER docking program used in ClusPro relies on the

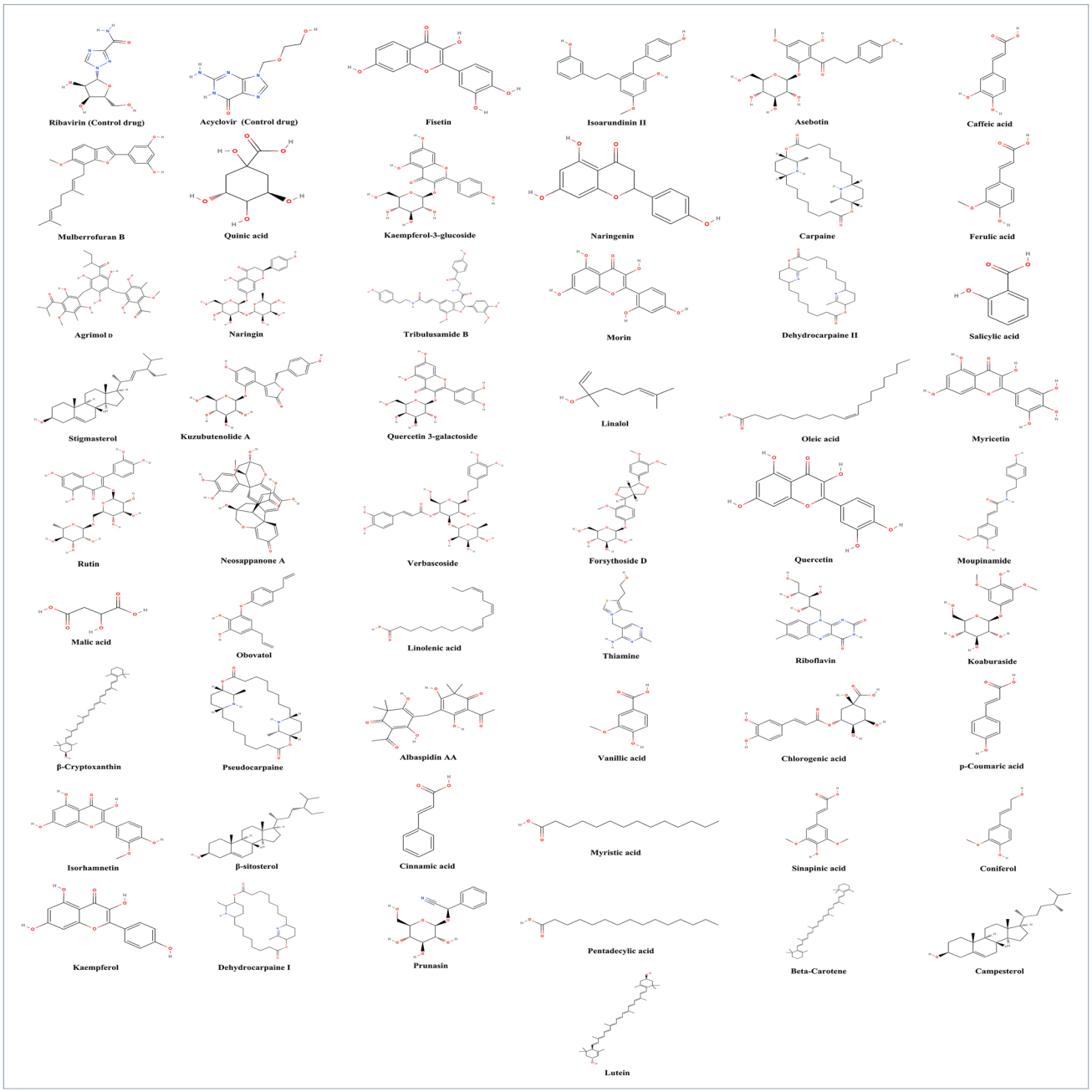


**Fig. 1** Two dimensional structures of the fifty-three phytochemicals, along with the control drugs (Ribavirin and Acyclovir)

Fast Fourier Transform correlation approach. The interaction energy between two proteins is represented by PIPER using the following expression;

$$E = w_1 E_{rep} + w_2 E_{attr} + w_3 E_{elec} + w_4 E_{DARS}$$

where the attractive and repulsive contributions to the van der Waals interaction energy are denoted by $E_{rep}$ and $E_{attr}$, electrostatic energy is denoted by $E_{elec}$, pairwise structure-based potential is represented by $E_{DARS}$ and the weights of the corresponding residues are determined by the coefficients $w_1$, $w_2$, $w_3$, and $w_4$ (Bhattacharya et al. 2020). PDBSum web server (http://www.ebi.ac.uk/pdbsum) was used to visualise and analyse interacting amino acids and bonds of the protein–protein complex (Laskowski 2009).

## Protein-phytochemical

Discovery Studio 2021 (BIOVIA, San Diego, USA) was used to predict the active sites in the receptor protein NiV G:A. The grid box encompassed GLN369A, GLU389A, TYR391A, and ILE398A residues (corresponds to GLN559, GLU579, TYR581, and ILE588 as per Kalbhor et al. 2021), which had a high binding affinity for Ephrin B2. The NiV G-Ephrin B2 complex was further used as a target protein for molecular docking studies with the phytochemicals and the control drugs, Ribavirin and Acyclovir. Ephrin B2 was also used as a target protein for molecular docking studies with the phytochemicals and the control drugs, Ribavirin and Acyclovir. The grid parameters for the respective receptor proteins are listed in Table 1. Protein-phytochemical molecular docking studies were performed by the DockThor web program (https://dockthor.lncc.br/v2/). DockThor uses Santos Dumont supercomputer (Santos et al. 2020) to conduct virtual screening experiments. It houses docking tools such as MMFF Ligand and PdbThorBox. The docking algorithm applies MMFF94S53 force field on the protein inputs (Nag et al. 2021a). The results of the protein–ligand docking studies (average of binding energies, Kcal $mol^{-1}$) were compared with that of the control drug complexes.

## Evaluation of drug-like properties and toxicity analysis

The pharmacological and drug-likeness properties of the phytochemicals were evaluated by uploading their canonical smile formats to the SwissADME site (http://www.swissadme.ch/). Drug likeness parameters, namely topological polar surface area (TPSA), lipophilicity (iLOGP and WLOGP), estimated water solubility (ESOL Log S), five rules of Lipinski, gastrointestinal (GI) absorption and PGP substrate, were used for evaluation of drug-likeness of the input phytocompounds. The efflux of structurally unrelated compounds is mediated by the membrane-bound transporter P-Glycoprotein (PGP), which alters the bioavailability of the drugs. The physicochemical property guideline of Lipinski's rule of five (RO5) should be followed by an ideal drug. As per RO5, a chemical compound with a certain biological activity for oral administration should have drug like properties like molecular weight less than 500 g $mol^{-1}$, log P (hydrophobicity) value less than 5, hydrogen bond donors less than or equal to 5 in numbers, and less than or equal to 10 hydrogen bond acceptor sites (Lipinski et al. 2001; Doak et al. 2014). SwissADME is an open-source web server that facilitates the drug discovery by predicting drug-likeness parameters. It also explores the physicochemical descriptors, and pharmacokinetic properties of the chemical entities (Daina et al. 2017). Toxicity can be attributed as one of the important reasons for the failure of the drug development pipeline. Hence, it is crucial to test the toxicity endpoints of compounds. The toxicological properties such as AMES toxicity, Rat Oral Acute Toxicity, Skin Sensitization and Respiratory Toxicity were evaluated using ADMETlab 2.0 web server (https://admetmesh.scbdd.com/) (Xiong et al. 2021).

## Principal component analysis and protein–ligand interaction analysis

Ten phytochemicals out of fifty-three total phytochemicals, along with the control drug, were selected based on the highest docking scores and evaluation of drug-likeness properties, which were then grouped by the application of Principal Component Analysis (PCA) using Minitab 18 statistical software. PCA simplifies the interpretation of large data sets by ensuring minimum loss of data sets, thereby improving data interpretation. The principal components depict an individual dimension of variations from the measured datasets. Principal components (PCs) are uncorrelated variables where PC1 encloses the maximum variation followed by PC2, PC3 and so on (Jolliffe and Cadima 2016; Lever et al. 2017). In this study, binding energy (Kcal $mol^{-1}$), molecular weights, and drug likeness

**Table 1** Grid parameters for protein–protein and protein–ligand docking studies

| Docking type | Center | | | Size | | |
|---|---|---|---|---|---|---|
| | X | Y | Z | X | Y | Z |
| Protein (NiV G-Ephrin B2)-Ligand docking | 5 | 66 | −3 | 20 | 20 | 20 |
| Protein (NiV G:A)-Ligand docking | 13.82 | 69.86 | −33.26 | | | |
| Protein (Ephrin B2)- Ligand docking | 5 | 66 | −3 | | | |

parameter values of the phytochemicals such as TPSA, iLOGP, WLOGP, ESOL Log S were used as inputs for the PCA. The outputs of PCA were observed as different clusters. The selection of one of the clusters for the molecular alignment study was done based on the presence of the phytochemical with the most optimum binding potentials to the active site of the target protein. The protein–ligand docking complexes associated with the phytochemicals of the selected cluster and the control drug were used for amino acid-ligand interaction analysis. The BIOVIA Discovery Studio Visualizer (Dassault Systems) software was used to visualise and analyse interacting amino acids and bonds of the protein-phytochemical complexes.

## Phytochemical alignment and identification of pharmacophores

Based on the multivariate PCA modelling results, the cluster comprising phytochemicals with the optimum binding affinity and drug-like properties was subjected to molecular alignment using an open-source server, PharmaGist (https://bioinfo3d.cs.tau.ac.il/PharmaGist/). The alignment of phytochemicals facilitated the identification of common descriptors or functional groups. PharmaGist utilizes the DUD (directory of useful decoys) data set, which consists of 2950 active ligands for 40 different receptors and 36 decoy compounds for active ligands. The alignment scores of the input ligands from the chosen PCA cluster were generated based on their pivot and conformational results after pairwise alignments (Schneidman-Duhovny et al. 2008). The output was chosen based on the highest alignment score. The analysis of the common descriptors (pharmacophores) responsible for effective ligand–protein interaction was performed by using ZincPharmer (http://zincpharmer.csb.pitt.edu/). The structures were visualized using PyMol 2.5 software (Schrödinger). PyMol is known to generate high-quality three-dimensional images of biological macromolecules, including proteins and small molecules. It includes OpenGL Extension Wrangler Library (GLEW) and FreeGLUT and is capable of solving Poisson-Boltzmann equations. It uses python as its programming language (Seeliger and de Groot 2010).

## Molecular dynamic (MD) simulation

The MD simulation of the NiV G:A and the phytochemical with the top binding affinity was performed using the GROMACS-2019.2 based bio-molecular package of Simlab, the University of Arkansas for Medical Sciences (UAMS), Little Rock, USA. The simulation utilised GROMOS96 43a1 force field. PRODRG software was used to generate the ligand topology file (Schüttelkopf and van Aalten 2004). A grid box was specified for the protein–ligand complex. An environment of SPC water and 0.15 M counter ions ($Na^+/Cl^-$) was specified for molecular dynamic simulation. The set-up parameters, NVT/NPT ensemble temperature 300 K and 1 bar atmospheric pressure were applied to the system. Parrinello-Rahmanbarostat and Parrinello-Danadio-Bussithermostat were used to maintain the pressure and temperature (Huang et al. 2017). Energy minimization by 5000 steepest descent integrators on the output model was performed. Based on the available literature (Tadayon and Garkani-Nejad 2019; Alamri et al. 2020; Keretsu et al. 2020; Basu et al. 2020; Kushwaha et al. 2021; Yadav et al. 2021; da Cruz Freire et al. 2022), the run time for the MD simulation was fixed at 50 ns.

The results of the MD simulation studies were expressed in terms of Root Mean Square Deviation (RMSD), Radius of Gyration (Rg), Root Mean Square Fluctuation (RMSF), and Ligand-H bonds. The measured distance between protein residues and ligands is determined by RMSD. The significance of the radius of gyration lies in the analysis of the compactness of the protein structure in the free and bound forms (Nag et al. 2023). RMSF represents the differences in flexibility among residues with respect to the average molecular dynamic simulation conformation (Rao et al. 2020). Additionally, a comparative analysis of structural changes between the ligand-bound and ligand-free proteins was performed by using PyMol measurement wizard.

## Free energy analysis by MM-PBSA (molecular mechanics-poisson–boltzmann solvent-accessible surface area) calculation

The free energies of the top ligand-NiV G:A complex were estimated by Molecular Mechanics-Poisson–Boltzmann Solvent-Accessible surface area (MM-PBSA) method using g-mmbsa package (Kumari et al. 2014; Nag et al. 2022a, b) for the final 10 ns of the simulation time frame. The free energy included ΔG_van der Waals, ΔG_Electrostatic, ΔG_Polar, ΔG_Non-Polar, ΔG_Binding and residual contribution energy parameters.

The calculation of ΔG_Bind (kJ $mol^{-1}$) was represented by the following equation:

$$\Delta G\_Bind = G\_Comp - (G\_Prot + G\_Lig)$$

The value of ΔG_Bind (kJ $mol^{-1}$) was derived by subtracting the summation of individual energy values of the protein (G_Prot) and ligand (G_Lig) from the energy of the protein–ligand complex (ΔG_Comp).

**Table 2** List of compounds selected for the study and its corresponding literature evidences

| Compound name | Rationale for selection |
|---|---|
| Ribavirin (Control drug) | Ribavirin was used as a control drug for the inhibition of viral entry, in vivo in BALB/c mice (Tang et al. 2019) |
| | Ribavirin was used to treat Nipah infection during past outbreak in Malaysia (Sharma et al. 2019) |
| | Ribavirin was found to inhibit Nipah virus glycoprotein in silico (Ghimire et al. 2022) |
| Naringin | Naringin was reported to have significant antiviral properties (Amin Huseen 2020) |
| | Naringin showed high binding affinity for the main protease of COVID-19 ($-10.2$ Kcal $mol^{-1}$) (Liu et al. 2022) |
| Tribulusamide B | Tribulusamide B showed hepatoprotective activity in mice (Li et al. 1998) |
| Mulberrofuran B | The anti-oxidant properties (ABTS and DPPH) of Mulberrofuran B were reported in the literature (Martins et al. 2021) |
| Rutin | Rutin showed inhibitory activities against infectious agents like Zika virus in *Escherichia coli* BL21 (DE3) (Lima et al. 2021) |
| Asebotin | Asebotin showed anti- H5N1 properties in vitro (Ibrahim et al. 2013) |
| Kaempferol-3-glucoside | In an in-silico study, Kaempferol-3-glucoside showed inhibitory properties against RNA-dependent RNA polymerase of the Japanese encephalitis virus (Yadav et al. 2022) |
| Kuzubutenolide A | Antiviral activity not reported |
| Fisetin | Molecular docking and simulation studies showed that Fisetin could strongly bind with the RNA-dependent RNA polymerase (RdRp) enzyme of Dengue virus in silico (Fatriansyah et al. 2022) |
| Naringenin | Naringenin (NAR) prevented Zika virus infection in human A549 cells, in vitro (Cataneo et al. 2019) |
| Morin | Morin showed antiviral activity against proteins of SARS-CoV-2, SARS-CoV and MERS-CoV in silico (Gupta et al. 2022) |
| Verbascoside | Verbascoside inhibited the expressions of antigens of hepatitis B virus in vitro in HepG2.2.15 and HL-7702 cells (Mou et al. 2021) |
| Forsythoside D | Forsythoside D had hepatoprotective and anti-hepatitis properties (Chakravarthy 2021) |
| Kaempferol | Kaempferol showed antiviral properties by suppressing the protein kinase B activity of SARS-CoV in Xenopus oocyte. The phytochemical is also known for having antioxidant and anti-inflammatory effects (Khazdair et al. 2021) |
| Carpaine | Carpaine through an in silico study showed inhibitory potential against dengue serotype 3 RNA-dependent RNA polymerase (RdRp) (Radhakrishnan et al. 2017) |
| Dehydrocarpaine II | Dehydrocarpaine II inhibited dengue serotype 3 RNA-dependent RNA polymerase, in silico (RdRp) (Radhakrishnan et al. 2017) |
| Dehydrocarpaine I | Dehydrocarpaine II inhibited dengue serotype 3 RNA-dependent RNA polymerase, in silico (RdRp) (Radhakrishnan et al. 2017) |
| Moupinamide | Moupinamide strongly inhibited Spike protein and the Main Protease activities of SARS-CoV-2 in silico (Shukla et al. 2021) |
| Agrimol D | Agrimol D possessed antiviral, antimicrobial and antioxidant properties (Le et al. 2018) |
| Koaburaside | Koaburaside has antioxidant, anti-HIV and anti-inflammatory properties (Choi et al. 2013) |
| Prunasin | Prunasin showed inhibitory properties against neo-coronavirus targets, Mpro and RdRp proteins in silico (Chen et al. 2022) |
| Neosappanone A | Neosappanone A showed inhibitory properties against Xanthine Oxidase and is considered useful in the treatment of gout (Pournaghi et al. 2020) |
| Obovatol | Obovatol exhibited anti-hepatitis B virus activities (Li et al. 2013) |
| Thiamine | Thiamine administration effectively reduced the hepatitis B virus DNA to undetectable levels in infected individuals (Wallace 2001) |
| Stigmasterol | Stigmasterol exhibited antiviral activity against dengue virus in vitro using Vero culture, cell line C6/36 culture (Soekamto et al. 2019) |
| Quercetin 3-galactoside | Quercetin-3-galactoside (Isoquercetin) had inhibitory properties against the viral spike protein of SARS-CoV-2 in silico (Jesus et al. 2020) |
| Quercetin | Quercetin showed anti-dengue property using Vero cells in vitro and protected mice (in vivo) from lethal infection of meningoencephalitis virus (Colunga Biancatelli et al. 2020) |
| Isoarundinin II | Antiviral activity not reported |
| Myricetin | Myricetin showed antioxidant, anticarcinogenic properties. It also exhibited potential antiviral behaviour against human immune-deficiency virus (Ong and Khoo 1997) |
| Linolenic acid | Linolenic acid showed anti-hepatitis B properties in vitro using Hep G2 2.2.15 cell line (Chou et al. 2012) |
| Pseudocarpaine | Pseudocarpaine showed strong binding affinity for receptor binding domain (RBD)-spike protein of SARS-CoV-2 in silico (Adel et al. 2022) |

**Table 2** (continued)

| Compound name | Rationale for selection |
|---|---|
| Isorhamnetin | Isorhamnetin exhibited inhibitory properties against the main protease of SARS-CoV-2 in silico (Shahhamzehei et al. 2022) |
| Oleic acid | Oleic acid showed anti-inflammatory bactericidal and fungicidal property (Sales-Campos et al. 2013) |
| Riboflavin | Riboflavin demonstrated antiviral activity by significantly lowering Middle-East respiratory syndrome coronavirus titer in the presence of ultraviolet light (Keflie and Biesalski 2021) |
| Chlorogenic acid | Chlorogenic acid inhibited Influenza A (H5N1) virus neuraminidase activity (Luo et al. 2011) |
| Coniferol | Coniferol exhibited anti-hepatitis B virus activity (Aguilar-Guadarrama and Rios 2018) |
| Beta-carotene | Beta-carotene was reported to enhance the immunity against virus and tumor surveillance (Fatima et al. 2014) |
| Campesterol | Campesterol showed anti-HIV property. It exhibited inhibitory properties against SARS-CoV-2 in silico (Jamhour et al. 2022) |
| β-sitosterol | β-sitosterol showed inhibitory properties against SARS-CoV-2 in silico (Khan and Siddiqui 2020) |
| Myristic acid | Myristic acid and its derivatives exhibited inhibitory properties against human immunodeficiency virus and hepatitis B virus in vitro (Parang et al. 1997) |
| Pentadecylic acid | Pentadecylic acid showed antioxidant, anti-inflammatory and anticancer properties (Sharma et al. 2014) |
| Ferulic acid | Ferulic acid showed inhibitory properties against SARS-CoV-2 in silico (Bhowmik et al. 2020) |
| Sinapinic acid | Sinapinic acid showed anti SARS-CoV-2 activity in vitro using Vero-E6 and in silico (Orfali et al. 2021) |
| Caffeic acid | Caffeic acid showed anti-hepatitis C property (Erdemli et al. 2015) |
| p-coumaric acid | The p-coumaric acid prolonged survival rates and reduced virus titers in bronchoalveolar lavage (BAL) fluids in mice model and showed anti-influenza activities (Pei et al. 2016) |
| Vanillic acid | Vanillic acid showed neuroprotective properties. Treatment with vanillic acid for 14 consecutive days in animal model (Bilateral Common Carotid Artery Occlusion and Reperfusion) restored with the spatial memory (Sharma et al. 2020) |
| Salicylic acid | Salicylic acid inhibited the SARS-CoV-2 activity in vero, Huh-7, and A549-ACE2 cell lines and in precision-cut, patient-derived lung slices (Geiger et al. 2022) |
| Cinnamic acid | Cinnamic acid showed inhibitory properties against Zika virus infection in vitro in Vero cells, Huh7 cells and A549 cells It successfully blocked the RNA-dependent RNA Polymerase activity. Cinnamic acid reduced the mortality in Zika virus infected type I/II interferon receptor-deficient (ifnagr–/–) C57BL/6 (AG6) mice in vivo (Chen et al. 2021) |
| Albaspidin AA | Albaspidin AA exhibited inhibitory activities against neuraminidase of Influenza virus (Xie et al. 2023) |
| Quinic acid | Quinic acid exhibited anti-hepatitis B activity in vitro in Hep G2.2.15 cells and in vivo in DHBV-infected duckling model (Wang et al. 2009) |
| β-Cryptoxanthin | β-cryptoxanthin exhibited inhibitory properties against main protease (Mpro) of SARS-CoV-2 in silico (Karpiński et al. 2021) |
| Linalol | Linalol exhibited anti-hepatitis B virus properties in vitro using 2.2.15 cell line derived from hepatoblastoma Hep G2 cells (Chiang et al. 2005) |
| Malic acid | Malic acid showed inhibitory properties against 3C-like main proteinase (3CLpro) and RNA-dependent RNA Polymerase proteins of SARS-CoV-2 in silico (Qazi et al. 2021) |
| Lutein | Lutein exhibited anti—hepatitis B virus activity by inhibition of hepatitis B virus transcription in stable HBV-producing human hepatoblastoma Hep G2 2.2.15 cells (Pang et al. 2010) |

## Results and discussion

### Selection of phytochemicals

Fifty-three phytochemicals, and the control drug Ribavirin were selected for this study based on literature studies mentioned in Table 2.

### Drug-likeness of selected compounds

The drug-like properties were effectively predicted by SwissADME for all the fifty-three phytochemicals, along with the control drugs, Ribavirin and Acyclovir (Table 3). The bioavailability of drug candidates was represented by Topological Polar Surface Area (TPSA). The suggested range is 20 to 140 $Å^2$ (Ertl et al. 2000). All the phytochemicals except for a few (Albaspidin AA, Beta-carotene, Chlorogenic acid, Riboflavin, Neosappanone A, Agrimol D, Forsythoside D, Verbascoside, Myricetin, Quercetin 3-galactoside, Kuzubutenolide A, Kaempferol-3-glucoside, Asebotin, Rutin, Mulberrofuran B) satisfied the criteria. Hou and Wang 2008, noted that in some cases, there might be no correlation between TPSA and other drug-like parameters. Water solubility also plays a vital role in determining drug-like properties. The solubility

**Table 3** Evaluation of drug-likeness of the phytochemicals as determined by SwissADME

| Molecule | Phytochemical name | TPSA | iLOGP | WLOGP | ESOL Log S | GI absorption | PgP substrate | Lipinski violations |
|---|---|---|---|---|---|---|---|---|
| Control drug | Ribavirin | 143.72 | 0.13 | −3.34 | −0.21 | Low | No | 0 |
| 1 | Acyclovir | 119.05 | 0.48 | −1.48 | −0.41 | High | No | 0 |
| 2 | Naringin | 109.64 | 2.68 | −4.13 | −2.70 | Low | Yes | 0 |
| 3 | Tribulusamide B | 73.22 | 3.00 | 2.92 | −3.80 | High | No | 0 |
| 4 | Mulberrofuran B | 256.29 | 2.08 | 0.29 | −5.24 | Low | Yes | 3 |
| 5 | Rutin | 269.43 | 1.58 | −1.69 | −3.3 | Low | Yes | 3 |
| 6 | Asebotin | 166.14 | 2.49 | 0.10 | −2.94 | Low | Yes | 1 |
| 7 | Kaempferol-3-glucoside | 190.28 | 0.53 | −0.24 | −3.18 | Low | No | 2 |
| 8 | Kuzubutenolide A | 166.14 | 1.75 | −0.17 | −2.90 | Low | Yes | 1 |
| 9 | Fisetin | 111.13 | 1.50 | 2.28 | −3.35 | High | No | 0 |
| 10 | Naringenin | 86.99 | 1.75 | 2.19 | −3.49 | High | Yes | 0 |
| 11 | Morin | 131.36 | 1.47 | 1.99 | −3.16 | High | No | 0 |
| 12 | Verbascoside | 245.29 | 3.00 | −1.12 | −2.87 | Low | Yes | 3 |
| 13 | Forsythoside D | 145.53 | 3.14 | 0.32 | −3.36 | Low | Yes | 2 |
| 14 | Kaempferol | 111.13 | 1.7 | 2.28 | −3.31 | High | No | 0 |
| 15 | Carpaine | 76.66 | 4.71 | 4.80 | −6.77 | High | No | 0 |
| 16 | Dehydrocarpaine II | 77.32 | 4.62 | 5.77 | −6.35 | High | Yes | 0 |
| 17 | Dehydrocarpaine I | 76.99 | 4.56 | 5.29 | −6.56 | High | Yes | 0 |
| 18 | Moupinamide | 78.79 | 2.58 | 2.37 | −3.03 | High | No | 0 |
| 19 | Agrimol D | 211.28 | 2.55 | 5.71 | −7.86 | Low | No | 3 |
| 20 | Koaburaside | 138.07 | 1.44 | −1.41 | −1.20 | Low | No | 0 |
| 21 | Prunasin | 123.17 | 1.27 | −1.26 | −1.17 | High | No | 0 |
| 22 | Neosappanone A | 183.21 | 1.71 | 1.37 | −4.17 | Low | No | 3 |
| 23 | Obovatol | 49.69 | 3.18 | 4.35 | −4.69 | High | No | 0 |
| 24 | Thiamine | 104.15 | −1.60 | 0.62 | −2.32 | High | Yes | 0 |
| 25 | Stigmasterol | 20.23 | 5.01 | 7.80 | −7.46 | Low | No | 1 |
| 26 | Quercetin 3-galactoside | 210.51 | 2.11 | −0.54 | −3.04 | Low | No | 2 |
| 27 | Quercetin | 131.36 | 1.63 | 1.99 | −3.16 | High | No | 0 |
| 28 | Isoarundinin II | 69.92 | 2.54 | 4.19 | −5.26 | High | No | 0 |
| 29 | Myricetin | 151.59 | 1.08 | 1.69 | −3.01 | Low | No | 1 |
| 30 | Linolenic acid | 37.30 | 3.36 | 5.66 | −4.78 | High | No | 1 |
| 31 | Pseudocarpaine | 76.66 | 4.71 | 4.80 | −6.77 | High | No | 0 |
| 32 | Isorhamnetin | 120.36 | 2.35 | 2.29 | −3.36 | High | No | 0 |
| 33 | Oleic acid | 37.30 | 4.27 | 6.11 | −5.41 | High | No | 1 |
| 34 | Riboflavin | 161.56 | 0.97 | −1.68 | −1.31 | Low | No | 0 |
| 35 | Chlorogenic acid | 164.75 | 0.96 | −0.75 | −1.62 | Low | No | 1 |
| 36 | Coniferol | 49.69 | 2.16 | 1.30 | −2.23 | High | No | 0 |
| 37 | Beta-carotene | 0.00 | 7.79 | 12.61 | −11.04 | Low | Yes | 2 |
| 38 | Campesterol | 20.23 | 4.92 | 7.63 | −7.54 | Low | No | 1 |
| 39 | β-sitosterol | 20.23 | 4.79 | 8.02 | −7.90 | Low | No | 1 |
| 40 | Myristic acid | 37.30 | 3.32 | 4.77 | −4.31 | High | No | 0 |
| 41 | Pentadecylic acid | 37.30 | 3.66 | 5.16 | −4.66 | High | No | 0 |
| 42 | Ferulic acid | 66.76 | 1.62 | 1.39 | −2.11 | High | No | 0 |
| 43 | Sinapinic acid | 75.99 | 1.63 | 1.40 | −2.16 | High | No | 0 |
| 44 | Caffeic acid | 77.76 | 0.97 | 1.09 | −1.89 | High | No | 0 |
| 45 | p-coumaric acid | 57.53 | 0.95 | 1.38 | −2.02 | High | No | 0 |
| 46 | Vanillic acid | 66.76 | 1.40 | 1.10 | −2.02 | High | No | 0 |
| 47 | Salicylic acid | 57.53 | 1.13 | 1.09 | −2.50 | High | No | 0 |

**Table 3** (continued)

| Molecule | Phytochemical name | TPSA | iLOGP | WLOGP | ESOL Log S | GI absorption | PgP substrate | Lipinski violations |
|---|---|---|---|---|---|---|---|---|
| 48 | Cinnamic acid | 37.30 | 1.55 | 1.68 | −2.37 | High | No | 0 |
| 49 | Albaspidin AA | 149.20 | 0.51 | 3.02 | −2.95 | Low | Yes | 0 |
| 50 | Quinic acid | 118.22 | −0.12 | −2.32 | 0.53 | Low | Yes | 0 |
| 51 | β-Cryptoxanthin | 20.23 | 7.44 | 11.58 | −10.33 | Low | Yes | 2 |
| 52 | Linalol | 20.23 | 2.70 | 2.67 | −2.40 | High | No | 0 |
| 53 | Malic acid | 94.83 | −0.01 | −1.09 | 0.32 | High | No | 0 |
| 54 | Lutein | 40.46 | 7.15 | 10.40 | −9.64 | Low | Yes | 2 |

*TPSA: Total Polar Surface Area; ESOL: Estimated Solubility; GI: Gastrointestinal; PgP: P-glycoprotein

for drugs calculated by applying the ESOL model should be less than 6. The linear relationship between log S and five molecular parameters, namely, molecular weight, the number of rotatable bonds, the fraction of heavy aromatic atoms and Daylight's CLOGP was established by the ESOL model (Daina et al. 2017). All the phytochemicals were found to be within the recommended ESOL Log S value. Absorbance in the gastrointestinal (GI) tract is representative of the transcellular passive diffusion parameter, which is crucial to the cellular permeability of the drug candidates (Nag et al. 2022b). In this study, compounds like Malic acid, Linalol, Cinnamic acid, Salicylic acid, Vanillic acid, p-Coumaric acid, Caffeic acid, Sinapinic acid, Ferulic acid, Pentadecylic acid, Myristic acid, Coniferol, Oleic acid, Isorhamnetin, Pseudocarpaine, Linolenic acid, Thiamine, Obovatol, Prunasin, Moupinamide, Dehydrocarpaine I, Dehydrocarpaine II, Carpaine, Kaempferol, Morin, Isoarundinin II, Quercetin, Naringenin, Fisetin, Acyclovir and Tribulusamide B showed high GI absorption capacity. The calculation of iLOGP is dependent upon the Gibbs free energy of solvation. The value of Gibbs free energy of solvation is derived from the ratio of Generalized-born (GB) parameters and solvent-accessible surface area in water/n-octanol (SA) (GB/SA). The iLOGP values for all the phytochemicals in this work, with exceptions to a few compounds (Stigmasterol, Beta-carotene, β-Cryptoxanthin, Lutein), were found to meet the recommended value (less than 5) (Ibrahim et al. 2021). The extra cellular efflux of a wide range of structurally unrelated drugs is mediated by membrane-bound transporter PGP (P-glycoprotein). PGP-induced efflux of various substrates against a concentration gradient lead to the decrease in the intracellular concentration of the substrates, impacting their oral bioavailability (Constantinides and Wasan 2007). Phytochemicals Lutein, β-Cryptoxanthin, Quinic acid, Albaspidin AA, Beta-carotene, Naringin, Thiamine, Dehydrocarpaine I, Mulberrofuran B, Dehydrocarpaine II, Forsythoside D, Verbascoside, Naringenin, Kuzubutenolide A, Asebotin and Rutin were found to be PGP substrate (PGP +), and rest were PGP negative. Minimum Lipinski violations (0–3) were observed for all the phytochemicals. In general, literature indicated that neither drug-likeness of a compound should be derived based on one parameter nor that a compound is expected to pass all the drug-like tests (Ertl et al. 2000). Based on this understanding, all the phytochemicals passed one or more criteria, and substantially established themselves as the candidate drugs.

The toxicity analysis of the selected compounds is presented in Table 4. Four test parameters, namely Ames test, rat oral acute toxicity, skin sensitization and respiratory toxicity were studied to evaluate the toxicity of the compounds. While the Ames test for mutagenicity represents carcinogenicity of the compounds, skin sensitization revealed conditions like allergies and diseases like contact dermatitis. Other test parameters such as rat oral acute toxicity and respiratory toxicity, are related to the morbidity and mortality. Surveillance and treatment of such parameters, should be given importance to avoid drug withdrawal (Dong et al. 2018; Xiong et al. 2021). The results indicated that most of the compounds selected in this study were safe and could be used as candidate drugs.

## Molecular docking

In the present study, docking results of all the fifty-three phytochemicals and the control drugs, Ribavirin and Acyclovir with the target protein (NiV G:A) were analysed (Table 5). However, the control drug, Acyclovir showed lower binding affinity (−6.55 kcal $mol^{-1}$) towards NiV G:A compared to Ribavirin (−6.95 kcal $mol^{-1}$). Literature showed the efficacy of Ribavirin against Nipah virus particles, in in vitro conditions (Wright et al. 2005; Aljofan et al. 2009). Acylovir, on the other hand, was administered to nine (9) Nipah-infected workers in Singapore; however, its role in curing the patients was unclear (Paton et al. 1999). Considering our current

**Table 4** Analysis of toxicity analysis of selected compounds as determined by ADMETlab 2.0 web server

The predicted output values of the toxicological parameters determined their probability of being toxic within a range of 0 to 1. An empirical decision taken based on the output categorized scores between 0 and 0.3 as excellent, 0.3–0.7 as medium and 0.7–1.0 as poor

| Molecule | Phytochemical name | AMES | Rat oral acute toxicity | Skin sensitization | Respiratory toxicity |
|---|---|---|---|---|---|
| Control drug | Ribavirin | 0.039 | 0.05 | 0.023 | 0.026 |
| 1 | Acyclovir | 0.866 | 0.279 | 0.483 | 0.949 |
| 2 | Naringin | 0.348 | 0.245 | 0.031 | 0.033 |
| 3 | Tribulusamide B | 0.235 | 0.114 | 0.905 | 0.049 |
| 4 | Mulberrofuran B | 0.01 | 0.032 | 0.792 | 0.763 |
| 5 | Rutin | 0.805 | 0.05 | 0.036 | 0.015 |
| 6 | Asebotin | 0.448 | 0.076 | 0.083 | 0.027 |
| 7 | Kaempferol-3-glucoside | 0.775 | 0.111 | 0.057 | 0.024 |
| 8 | Kuzubutenolide A | 0.719 | 0.452 | 0.026 | 0.033 |
| 9 | Fisetin | 0.73 | 0.178 | 0.919 | 0.074 |
| 10 | Naringenin | 0.342 | 0.694 | 0.925 | 0.34 |
| 11 | Morin | 0.616 | 0.053 | 0.87 | 0.057 |
| 12 | Verbascoside | 0.389 | 0.094 | 0.687 | 0.015 |
| 13 | Forsythoside D | 0.268 | 0.15 | 0.036 | 0.037 |
| 14 | Kaempferol | 0.672 | 0.156 | 0.856 | 0.09 |
| 15 | Carpaine | 0.012 | 0.045 | 0.877 | 0.941 |
| 16 | Dehydrocarpaine II | 0.025 | 0.056 | 0.964 | 0.918 |
| 17 | Dehydrocarpaine I | 0.015 | 0.027 | 0.944 | 0.933 |
| 18 | Moupinamide | 0.228 | 0.269 | 0.94 | 0.475 |
| 19 | Agrimol D | 0.043 | 0.012 | 0.966 | 0.022 |
| 20 | Koaburaside | 0.309 | 0.058 | 0.084 | 0.04 |
| 21 | Prunasin | 0.631 | 0.321 | 0.173 | 0.973 |
| 22 | Neosappanone A | 0.583 | 0.889 | 0.856 | 0.915 |
| 23 | Obovatol | 0.121 | 0.077 | 0.956 | 0.479 |
| 24 | Thiamine | 0.008 | 0.064 | 0.25 | 0.684 |
| 25 | Stigmasterol | 0.029 | 0.054 | 0.025 | 0.19 |
| 26 | Quercetin 3-galactoside | 0.809 | 0.073 | 0.163 | 0.025 |
| 27 | Quercetin | 0.657 | 0.065 | 0.919 | 0.072 |
| 28 | Isoarundinin II | 0.137 | 0.115 | 0.946 | 0.051 |
| 29 | Myricetin | 0.482 | 0.022 | 0.943 | 0.065 |
| 30 | Linolenic acid | 0.113 | 0.005 | 0.965 | 0.674 |
| 31 | Pseudocarpaine | 0.012 | 0.045 | 0.877 | 0.941 |
| 32 | Isorhamnetin | 0.596 | 0.074 | 0.774 | 0.121 |
| 33 | Oleic acid | 0.004 | 0.016 | 0.951 | 0.704 |
| 34 | Riboflavin | 0.046 | 0.025 | 0.01 | 0.216 |
| 35 | Chlorogenic acid | 0.026 | 0.028 | 0.156 | 0.031 |
| 36 | Coniferol | 0.141 | 0.386 | 0.949 | 0.502 |
| 37 | Beta-carotene | 0.128 | 0.132 | 0.988 | 0.313 |
| 38 | Campesterol | 0.032 | 0.023 | 0.176 | 0.502 |
| 39 | β-sitosterol | 0.026 | 0.018 | 0.133 | 0.536 |
| 40 | Myristic acid | 0.006 | 0.037 | 0.807 | 0.807 |
| 41 | Pentadecylic acid | 0.005 | 0.033 | 0.869 | 0.873 |
| 42 | Ferulic acid | 0.114 | 0.733 | 0.929 | 0.72 |
| 43 | Sinapinic acid | 0.016 | 0.321 | 0.949 | 0.428 |
| 44 | Caffeic acid | 0.183 | 0.833 | 0.942 | 0.422 |
| 45 | p-coumaric acid | 0.045 | 0.796 | 0.941 | 0.512 |

**Table 4** (continued)

The predicted output values of the toxicological parameters determined their probability of being toxic within a range of 0 to 1. An empirical decision taken based on the output categorized scores between 0 and 0.3 as excellent, 0.3–0.7 as medium and 0.7–1.0 as poor

| Molecule | Phytochemical name | AMES | Rat oral acute toxicity | Skin sensitization | Respiratory toxicity |
|---|---|---|---|---|---|
| 46 | Vanillic acid | 0.015 | 0.053 | 0.154 | 0.12 |
| 47 | Salicylic acid | 0.018 | 0.516 | 0.288 | 0.897 |
| 48 | Cinnamic acid | 0.07 | 0.14 | 0.951 | 0.624 |
| 49 | Albaspidin AA | 0.018 | 1.0 | 0.046 | 0.727 |
| 50 | Quinic acid | 0.031 | 0.011 | 0.031 | 0.019 |
| 51 | β-Cryptoxanthin | 0.146 | 0.133 | 0.986 | 0.487 |
| 52 | Linalol | 0.006 | 0.02 | 0.631 | 0.039 |
| 53 | Malic acid | 0.02 | 0.009 | 0.264 | 0.394 |
| 54 | Lutein | 0.359 | 0.193 | 0.971 | 0.357 |

results and lack of evidence in the literature for anti-Nipah drugs, Ribavirin was used as the control drug in our study.

The evaluation of the top ten (10) docking scores showed that phytochemicals (Naringin, Tribulusamide B, Mulberrofuran B, Rutin, Asebotin, Kaempferol-3-glucoside, Kuzubutenolide A, Fisetin, Naringenin, Quercetin 3-galactoside) could strongly bind with the target NiV G:A (−9.19, −9.01, −8.84, −8.71, −8.56, −8.51, −8.32, −8.28, −8.25, −8.23 kcal $mol^{-1}$, respectively) when compared with the control drug, Ribavirin. The medicinal importance of these compounds is tabulated in Table 2. However, only two compounds namely, Naringin and Tribulusamide B showed a binding affinity of more than 9 kcal $mol^{-1}$, compared with other top-ranked phytochemicals. However, in the toxicity analysis of our study, Naringin was found to be safer than Tribulusamide B. Additionally, the affinity of phytochemicals towards the Ephrin B2-NiV G:A and human Ephrin B2 protein alone, were also evaluated (Tables S1 and S2). The result indicated that the top ligand Naringin, in particular, could selectively bind with NiV G:A (−9.19 kcal $mol^{-1}$) and NiV G-Ephrin B2 complex (−10.27 kcal $mol^{-1}$) over human Ephrin B2 protein alone (−7.09 kcal $mol^{-1}$). However, Naringin showed higher affinity towards Ephrin B2, than the control drug Ribavirin (−6.974 kcal $mol^{-1}$). Ephrin B2 is a B-class ephrin and potential henipaviral receptor, which facilitates viral entry and activates the virus-host fusion (Priyadarsinee et al. 2022). Naringin was reported to have significant anti-viral properties. In a recent study, Hussen et al. (2020), through molecular studies, showed that Naringin with binding affinity −10.2 kcal $mol^{-1}$, could strongly inhibit the activity of SARS-CoV-2 main protease (Amin Huseen 2020). Our result showed that the phytochemical Naringin could effectively disrupt NiV G: A-Ephrin B2 complex. Due to its comparative selectivity towards viral protein than the human receptor, post-infection clearance shall be possible. The three-dimensional structures of Naringin-protein complexes are shown in Fig. 2.

## Principal component analysis

In this work, the first principal component (PC1) and the second component (PC2) explained approximately 49.70 and 24.20% of the variance, respectively. We observed four clusters in the PCA (Fig. 3). Cluster 4 consisted of Naringin, Quercetin 3-galactoside, Rutin and Mulberrofuran B, while cluster 1, comprised the control drug Ribavirin along with Kaempferol-3-glucoside and Kuzubutenolide A. Fisetin and Naringenin were observed in cluster 2 and Asebotin and Tribulusamide B were grouped into cluster 3. There were marginal differences observed concerning the selected parameters (binding affinities and drug-likeness parameters) for clusters 3 and 4. Clusters 3 and 4 grouped top-ranked ligands in binding affinities towards NiV G:A, which also had higher molecular weights, and similar ranges of values for iLOGP and ESOL Log S, respectively. Clusters 1 and 2 consisted of low-scoring ligands in binding affinities towards NiV G:A, which also had differences in molecular weights, WLOGP, iLOGP, and ESOL Log S. The TPSA values for phytochemicals of cluster 4 were the highest, followed by cluster 3, 1 and 2. The observed differences associated with selected parameters for cluster 1 and 2 were more when compared to the differences related to the parameters for clusters 3 and 4. The multidimensional data analysis tool of Principal Component Analysis (PCA) can be used to achieve insightful information on the protein–ligand binding affinities (Nag et al. 2022b). The molecular interactions of Mur enzymes of *Mycobacterium tuberculosis* by utilizing the advanced PCA tool were explored by Kumari et al. 2021. The uniqueness of PCA lies in the conversion of measured variables into principal components. The use of the PCA tool for categorization

**Table 5** The results of molecular docking in terms of binding affinity (kcal $mol^{-1}$) between compounds and target protein as generated by the DockThor server

| PubChem Id (CID) | Compounds | Phytochemical class | Binding affinity (kcal $mol^{-1}$) |
|---|---|---|---|
| 37542 | Ribavirin (Control drug) | Triazole ribonucleosides and ribonucleotides | −6.95 |
| 442428 | Naringin | Flavonoids | **−9.19** |
| 10394345 | Tribulusamide B | 2-arylbenzofuran flavonoids | −9.01 |
| 6440635 | Mulberrofuran B | 2-arylbenzofuran flavonoids | −8.84 |
| 5280805 | Rutin | Flavonoids | −8.71 |
| 11190157 | Asebotin | Flavonoids | −8.56 |
| 5282102 | Kaempferol-3-glucoside | Flavonoids | −8.51 |
| 10671648 | Kuzubutenolide A | Organooxygen compounds | −8.32 |
| 5281614 | Fisetin | Flavonoids | −8.28 |
| 932 | Naringenin | Flavonoids | −8.25 |
| 5281643 | Quercetin 3-galactoside | Flavonoids | −8.23 |
| 5280343 | Quercetin | Flavonoids | −8.20 |
| 91542987 | Isoarundinin II | Stilbenes | −8.19 |
| 5281672 | Myricetin | Flavonoids | −8.08 |
| 5281670 | Morin | Flavonoids | −7.97 |
| 5281800 | Verbascoside | Cinnamic acids and derivatives | −7.91 |
| 24721571 | Forsythoside D | Lignan glycosides | −7.87 |
| 5280863 | Kaempferol | Flavonoids | −7.85 |
| 442630 | Carpaine | Macrolides and analogues | −7.82 |
| 131750992 | Dehydrocarpaine II | Macrolides and analogues | −7.80 |
| 131750991 | Dehydrocarpaine I | Macrolides and analogues | −7.75 |
| 5280537 | Moupinamide | Cinnamic acids and derivatives | −7.69 |
| 102402554 | Agrimol D | Diarylheptanoids | −7.68 |
| 5318820 | Koaburaside | Organooxygen compounds | −7.68 |
| 119033 | Prunasin | Organooxygen compounds | −7.67 |
| 101353537 | Neosappanone A | Tetralins | −7.58 |
| 100771 | Obovatol | Benzene and substituted derivatives | −7.51 |
| 1130 | Thiamine | Diazines | −7.39 |
| 5280794 | Stigmasterol | Steroids and steroid derivatives | −7.37 |
| 5280934 | Linolenic acid | Fatty Acyls | −7.35 |
| 12305270 | Pseudocarpaine | Macrolides and analogues | −7.33 |
| 5281654 | Isorhamnetin | Flavonoids | −7.27 |
| 445639 | Oleic acid | Fatty Acyls | −7.26 |
| 493570 | Riboflavin | Pteridines and derivatives | −7.21 |
| 1794427 | Chlorogenic acid | Organooxygen compounds | −7.03 |
| 1549095 | Coniferol | Phenols | −7.02 |
| 5280489 | Beta-carotene | Prenol lipids | −7.02 |
| 173183 | Campesterol | Steroids and steroid derivatives | −7.00 |
| 222284 | β-sitosterol | Steroids and steroid derivatives | −7.00 |
| 11005 | Myristic acid | Fatty Acyls | −6.65 |
| 13849 | Pentadecylic acid | Fatty Acyls | −6.64 |
| 445858 | Ferulic acid | Cinnamic acids and derivatives | −6.58 |
| 637775 | Sinapinic acid | Cinnamic acids and derivatives | −6.58 |
| 689043 | Caffeic acid | Cinnamic acids and derivatives | −6.50 |
| 637542 | p-coumaric acid | Cinnamic acids and derivatives | −6.48 |
| 8468 | Vanillic acid | Benzene and substituted derivatives | −6.47 |
| 338 | Salicylic acid | Benzene and substituted derivatives | −6.44 |

**Table 5** (continued)

| PubChem Id (CID) | Compounds | Phytochemical class | Binding affinity (kcal $mol^{-1}$) |
|---|---|---|---|
| 444539 | Cinnamic acid | Cinnamic acids and derivatives | −6.40 |
| 14378646 | Albaspidin AA | Vinylogous acids | −6.38 |
| 6508 | Quinic acid | Organooxygen compounds | −6.32 |
| 5281235 | β-Cryptoxanthin | Prenol lipids | −6.09 |
| 6549 | Linalol | Prenol lipids | −5.99 |
| 525 | Malic acid | Hydroxy acids and derivatives | −5.98 |
| 5281243 | Lutein | Prenol lipids | −3.08 |

*The highest binding affinity (−9.19 kcal $mol^{-1}$) associated with Naringin has been marked as bold

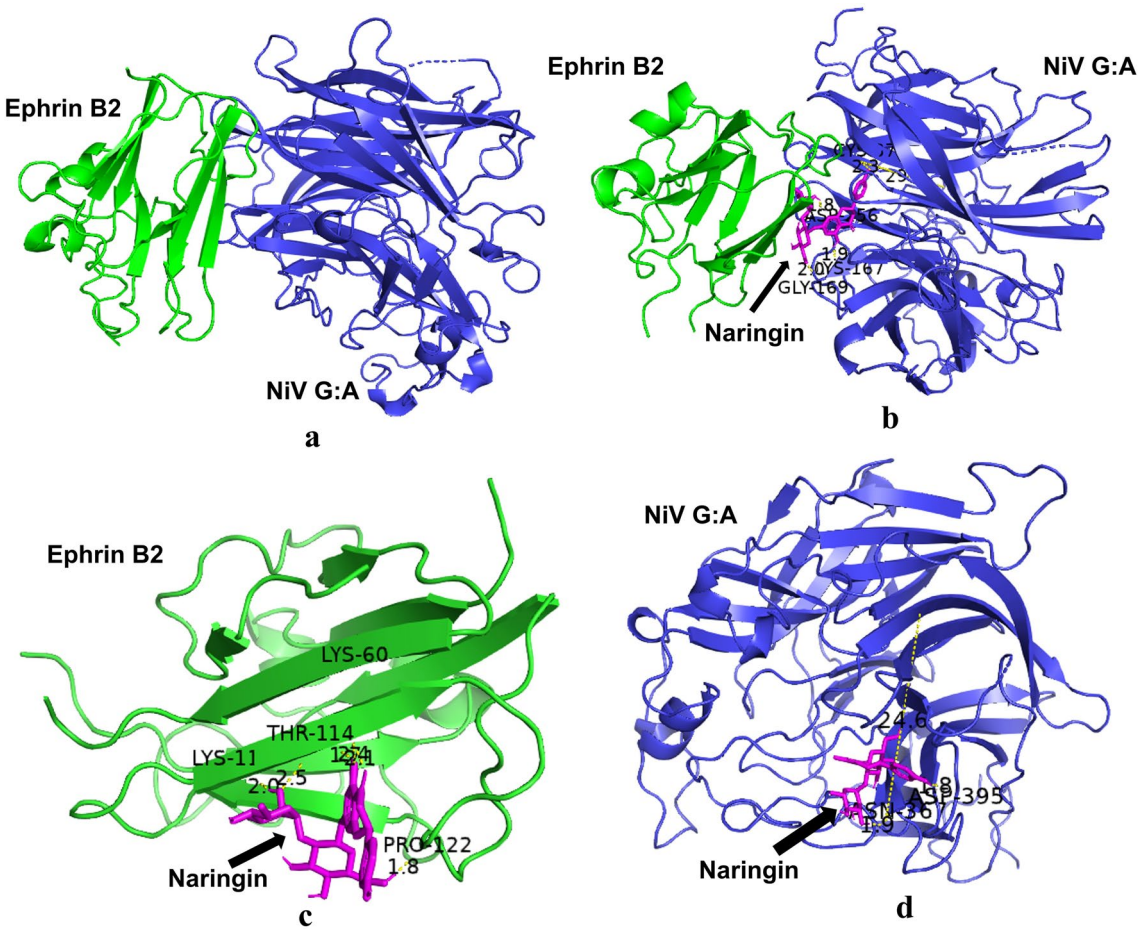


**Fig. 2** Three-dimensional structures of ligand–protein complexes. **a** Nipah virus attachment glycoprotein (NiV G:A) in complex with Ephrin B2 (PDB id 2VSM) **b** NiV G:A-Ephrin B2-Naringin complex **c** Ephrin B2-Naringin complex **d** NiV G:A-Naringin complex

of ligands and thereby establishing a correlation between the ligands was successfully implemented in our previous works (Nag et al. 2021a, 2022b, 2023). Considering the robustness of the PCA tool and based on our results, the compounds in cluster 4 were selected for pharmacophore study.

## Interaction analysis

PCA cluster 4, ligands-NiV G:A and Ephrin B2 docked complexes were selected for the amino acid-ligand interaction analysis (Fig. 4). The phytochemicals, Naringin, Rutin,

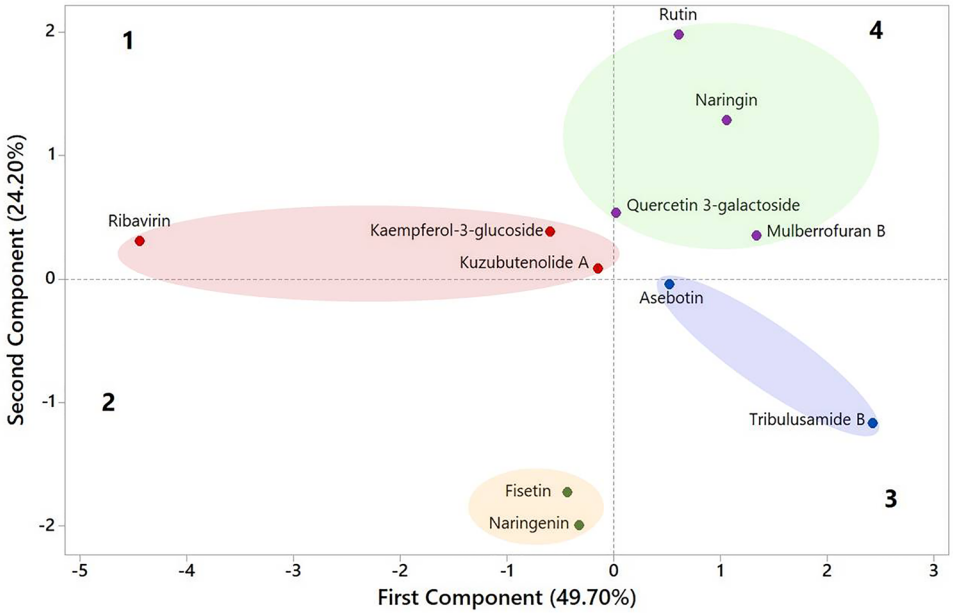


**Fig. 3** Principal Component Analysis of selected top ten phytochemicals showing four clusters (1, 2, 3 and 4), x and y axis represents First and Second components respectively

Mulberrofuran B and Quercetin 3-galactoside interacted with the amino acid residues of the target protein through conventional hydrogen bonds, carbon-hydrogen bonds, alkyl bonds, pi-pi t shaped bonds and pi-sulfur bonds. Some residues GLN369A, GLU389A, TYR391A, and ILE398A (corresponds to GLN559, GLU579, TYR581, and ILE588 as per Kalbhor et al. 2021) involved with the interactions had a strong binding affinity towards Ephrin B2. The control drug, Ribavirin, interacted with NiV G:A through conventional hydrogen, pi-sulfur, pi-alkyl and pi-pi t shaped bonds. Among various amino acids, ALA342A and CYS50A of NiV G:A were found to be the common residues omnipresent in all interactions, including the control drug, Ribavirin. For Ephrin B2, two amino acid residues THR114B, and LYS60B were found to be common when compared with the control drug, Ribavirin. The details of the ligand–protein interactions are presented in Table 6. Further, the comparative interactions between the top ligand Naringin-NiV G:A-Ephrin B2 and NiV G:A-Ephrin B2 complexes revealed GLU36A and PRO122B as the common residues. Also, Naringin was found to be placed within the attachment site of NiV G:A and Ephrin B2 (PHE376A, LEU377A, LEU378A, LYS379A; GLY37A, TYR38A; LYS116B, GLN118B, GLU119B, PHE120B, SER121B; SER257A, LEU258A) (Fig. S1).

## Phytochemical alignment and identification of pharmacophores

Based on the PCA results, as explained earlier, cluster 4 (Naringin, Rutin, Mulberrofuran B and Quercetin 3-galactoside) was selected for the pharmacophore (descriptors) dependent molecular alignment. Phytochemical alignment reveals molecular features responsible for the biological properties of the drug. The functional descriptors include hydrogen bond donors (HBD), hydrogen bond acceptors (HBA), positive features, negative features, aromatic rings and hydrophobic features (Mohammed 2021). The interactions with the target proteins are carried out by the descriptors present in the ligands. In our recent study, a similar technique was used to align phytochemicals based on the descriptors in *Camelia sinensis* L. (Nag et al. 2022b).

Further, we successfully deployed molecular alignment elsewhere to evaluate the interaction of the phytochemicals with the residues of the target protein (Nag et al. 2021b, 2023; Nag and Banerjee 2021). All these studies combined PCA and molecular alignment. Recently, Glaab et al. 2021 performed pharmacophore modelling-based study which involved molecular alignment of ligands to virtually screen SARS-CoV-2 viral protease $3CL^{pro}$ inhibitors from ZINC database, SWEETLEAD library and MolPort library. In the current study, we identified common descriptors for all cluster 4 phytochemicals as four H bond acceptors, one H bond donor and two aromatic groups (Fig. 5a), with a high alignment score of 32.245, as provided by the PharmaGist webserver. While evaluating the interacting groups of the ligands with the target proteins, we observed that identified common descriptors of Naringin, Rutin, Mulberrofuran B and Quercetin 3-galactoside were the functional pharmacophores responsible for the protein–ligand interaction, as shown in Fig. 5b.

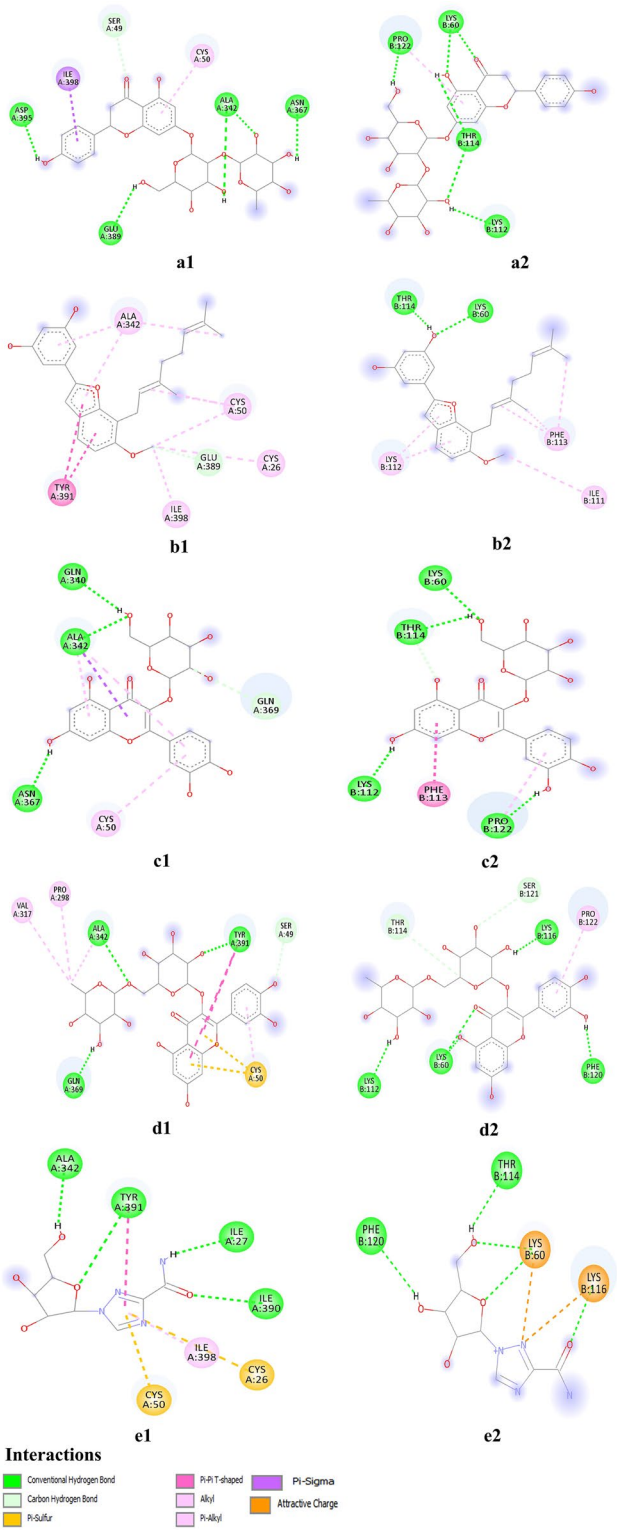


**Fig. 4** Two-dimensional representation of protein–ligand interactions (PCA cluster 4): **a1** to **e1** Interaction with Nipah virus attachment glycoprotein (NiV G:A, PDB id 2VSM, Chain A) [**a1** Naringin, **b1** Mulberrofuran B, **c1** Quercetin 3-galactoside, **d1** Rutin, **e1** Ribavirin]; **a2** to **e2** Interaction with Ephrin B2 (PDB id 2VSM, Chain B) [**a2** Naringin, **b2** Mulberrofuran B, **c2** Quercetin 3-galactoside, **d2** Rutin, **e2** Ribavirin]

## Molecular dynamic (MD) simulation

The molecular dynamic simulation tool is commonly used to validate the conformation and molecular stability of the docked complexes in physiological conditions (Dhiman and Purohit 2022). In the present study, MD simulation tool was used to examine the stability and conformational dynamics of the top ranked Naringin-NiV G:A complex. The stability of the complex was compared with that of the Ribavirin-NiV G:A in terms of results obtained collectively from all four parameters, namely RMSD, RMSF, gyration and ligand–protein H bonds. The binding profiles for the control drug Ribavirin and Naringin to the target protein, as demonstrated by the results, were similar. The application of the MD simulation technique is widespread in literature. Kumar et al. (2023) recently evaluated quinoline molecules mediated structure restoration and aggregate inhibition of V30M mutant transthyretin protein by applying a robust MD simulation technique. In another study, with the effective utilization of this technique, Singh and Purohit (2023) screened thirty-two 3-methyleneisoindolin-1-one molecules, and M24 was reported as the top cyclin-dependent kinases 4/6 (CDK4/6) inhibitor in comparison with the drug Palbociclib. The average RMSD values of the native complexes were 0.26, 0.24 and 0.23 nm for apo, Ribavirin-NiV G:A and Naringin-NiV G:A, respectively. Minimal fluctuations of RMSD (around ± 0.05 nm) for both the complexes observed were comparable to that of the apo (ligand free) protein (Fig. 6a). Literature indicated that RMSD value less than 2 Å represented the stability of protein structure, which in turn could be translated as less deviation of protein (Singh et al. 2022). Further, scientific evidence indicated that conformational changes resulting from protein–ligand interactions impacted the RMSD values, and thereby slight fluctuations in the RMSD profiles were expected during the simulation study (Alamri et al. 2020). Randhawa et al. (2022), in a five (5) ns simulation, established stability of the docked Nipah protein and selected phytochemical complexes. RMSD fluctuations during the simulation, were also observed in their study. Overall, our results in terms of RMSD for both the complexes and the apo protein, were in agreement with these literal evidences, indicating the stability of ligand–protein complexes in our study.

The Rg values ranged from 1.67 to 1.70 nm, demonstrating that the compactness of the protein was not impacted by ligand binding (Fig. 6b). We observed limited fluctuation of the ligand-bound (Naringin) protein gyration near 30–40 ns intervals. Minor fluctuations of the radius of gyration have been commonly observed in biological systems. In an in silico molecular dynamic simulation study of ATP-binding cassette super-family G member 2 enzyme and 2,4-Disubstituted pyridopyrimidine derivatives, lower fluctuations in the radius of gyration between 45 and 50 ns were reported

**Table 6** Amino acid residues of target proteins interacting with the phytochemicals

| Name (PubChem CID) | Nipah virus attachment glycoprotein (NiV G:A) | | | | Ephrin B2 | | | |
|---|---|---|---|---|---|---|---|---|
| | Amino acid interactions | Hydrogen bonds/ carbon hydrogen bonds | Alkyl bonds | Other bonds | Amino acid interactions | Hydrogen bonds/ carbon hydrogen bonds | Alkyl bonds | Other bonds |
| Ribavirin (37542) | **ALA342A**, TYR391A, ILE27A, ILE390A, CYS26A, **CYS50A** | **ALA342A,** ILE27A, ILE390A, TYR391A | ILE398A | CYS26A, **CYS50A,** TYR391A | PHE120B, **THR114B**, **LYS60B**, LYS116B | PHE120B, **THR114B**, **LYS60B**, LYS116B | – | **–LYS60B,** LYS116B |
| Naringin (442428) | **ALA342A**, ASN367A, GLU389A, ASP395A, ILE398A, **CYS50A**, SER49 | **ALA342A,** ASN367A, GLU389A, ASP395A, SER49 | **CYS50A** | ILE398A | PRO122B, **LYS60B**, **THR114B**, LYS112B | PRO122B, **LYS60B**, **THR114B,** LYS112B | PRO122B | – |
| Mulberrofuran B (6440635) | **ALA342A**, **CYS50A**, CYS26A, ILE398A, GLU389A, TYR391A | GLU389A | **ALA342A, CYS50A,** CYS26A, ILE398A | TYR391A | **THR114B**, **LYS60B**, PHE113B, ILE111B, LYS112B | **THR114B, LYS60B** | PHE113B, ILE111B, LYS112B | – |
| Rutin (5280805) | VAL317A, PRO298A, **ALA342A**, TYR391A, SER49A, **CYS50A**, GLN369A | SER49A, TYR391A, GLN369A, **ALA342A** | **CYS50A, ALA342A,** PRO298A, VAL317A | **CYS50A,** TYR391A | **THR114B**, SER121B,LYS116B,PRO122B, PHE120B, **LYS60B**, LYS112B | **THR114B,** SER121B,LYS116B, PHE120B, **LYS60B**, LYS112B | PRO122B, | – |
| Quercetin 3-galactoside (5281643) | ASN367A, **CYS50A**, **ALA342A**, GLN369A, GLN340A | ASN367A, GLN369A, GLN340A, **ALA342A** | **CYS50A, ALA342A** | **ALA342A** | **LYS60B**, **THR114B**, LYS112B, PHE113B, PRO122B | **LYS60B**, **THR114B**, LYS112B, PRO122B | PRO122B | PHE113B |

**The common residues for NiV G:A (ALA342A and CYS50A) are marked as bold. The common residues for Ephrin B2 (LYS60B and THR114B) are marked as bold

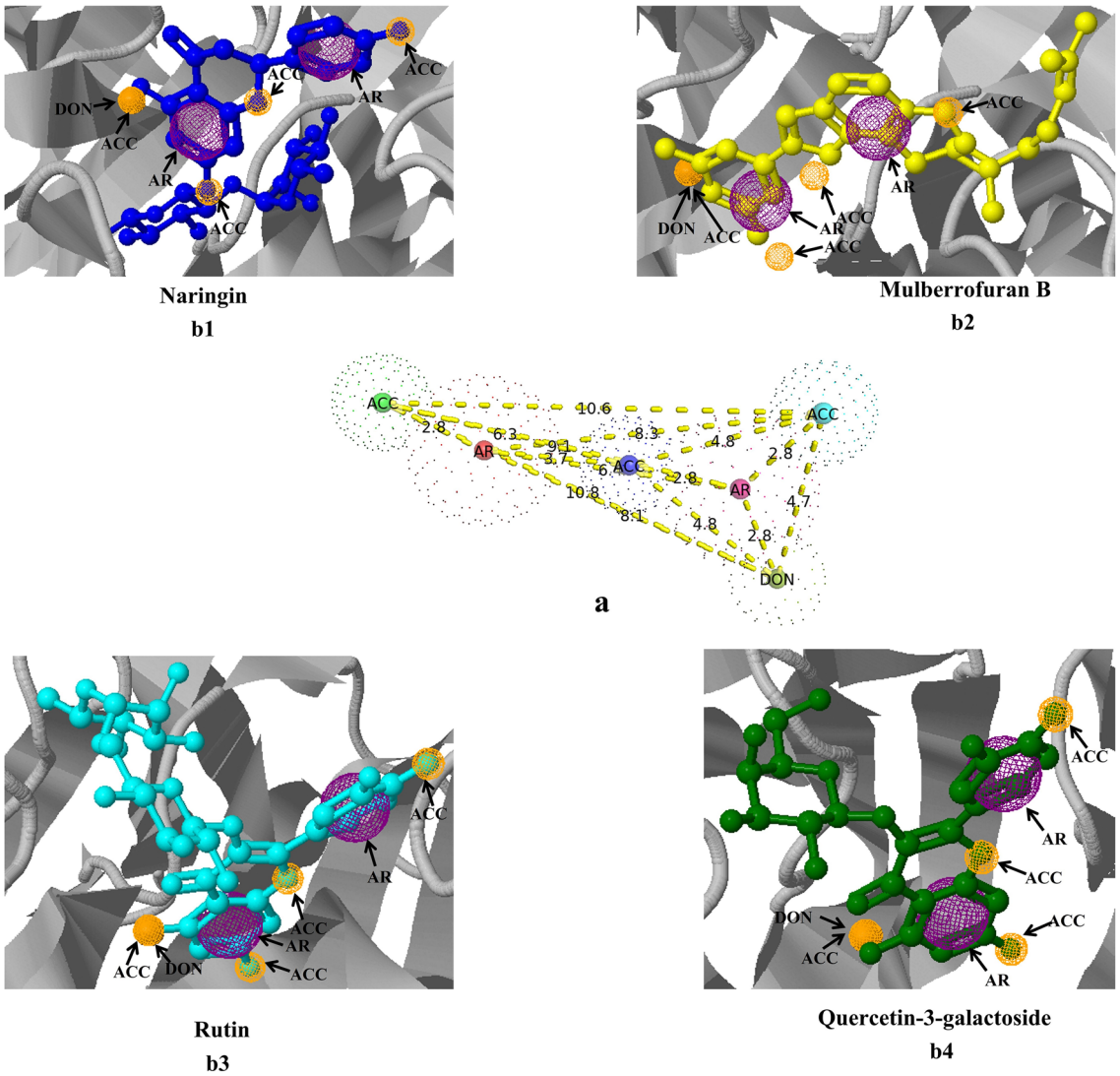


**Fig. 5** Molecular alignment of phytochemicals and pharmacophore interactions, **a** Identification of pharmacophores of four aligned phytochemicals (Naringin, Mulberrofuran B, Rutin and Quercetin 3 galactoside); **b1-b2-b3-b4** Three-dimensional representation of protein–ligand pharmacophores interactions (ACC: Acceptor, DON: Donor, AR: Aromatic)

(Tadayon and Garkani-Nejad 2019). Such fluctuations in RMSD and Rg parameters were reported elsewhere (Hasan et al. 2022). The root mean square fluctuations (RMSF) of individual amino acid residues was analysed to understand the residual mobility of ligand-bound and unbound forms (Kumar et al. 2023). The average RMSF values for apo-protein, Naringin-NiV G:A and Ribavirin-NiV G:A ranged from 0.1 to 0.5 nm (Fig. 6c). The structural stability of the complex is affected by the formation of stable hydrogen bonds between ligand and protein. For interaction with the NiV G:A, Naringin and Ribavirin showed a maximum of six and four hydrogen bonds, respectively. We observed at least one hydrogen was long-lived throughout the simulation of 50 ns for both the Naringin and Ribavirin complexes (Fig. 6d). The molecular docking simulation study results showed that Naringin could make an effective and stable interaction with the target protein NiV G:A at its active site and, thereby, could inhibit the Nipah Virus infection.

## Free energy analysis by MM-PBSA calculation

In agreement with our molecular docking result, free energy analysis showed that Naringin (−218.664 kJ $mol^{-1}$) had a higher binding affinity to that of the control drug, Ribavirin (−83.812 kJ $mol^{-1}$). Low binding energy in MM-PBSA analysis represents a strong binding potential

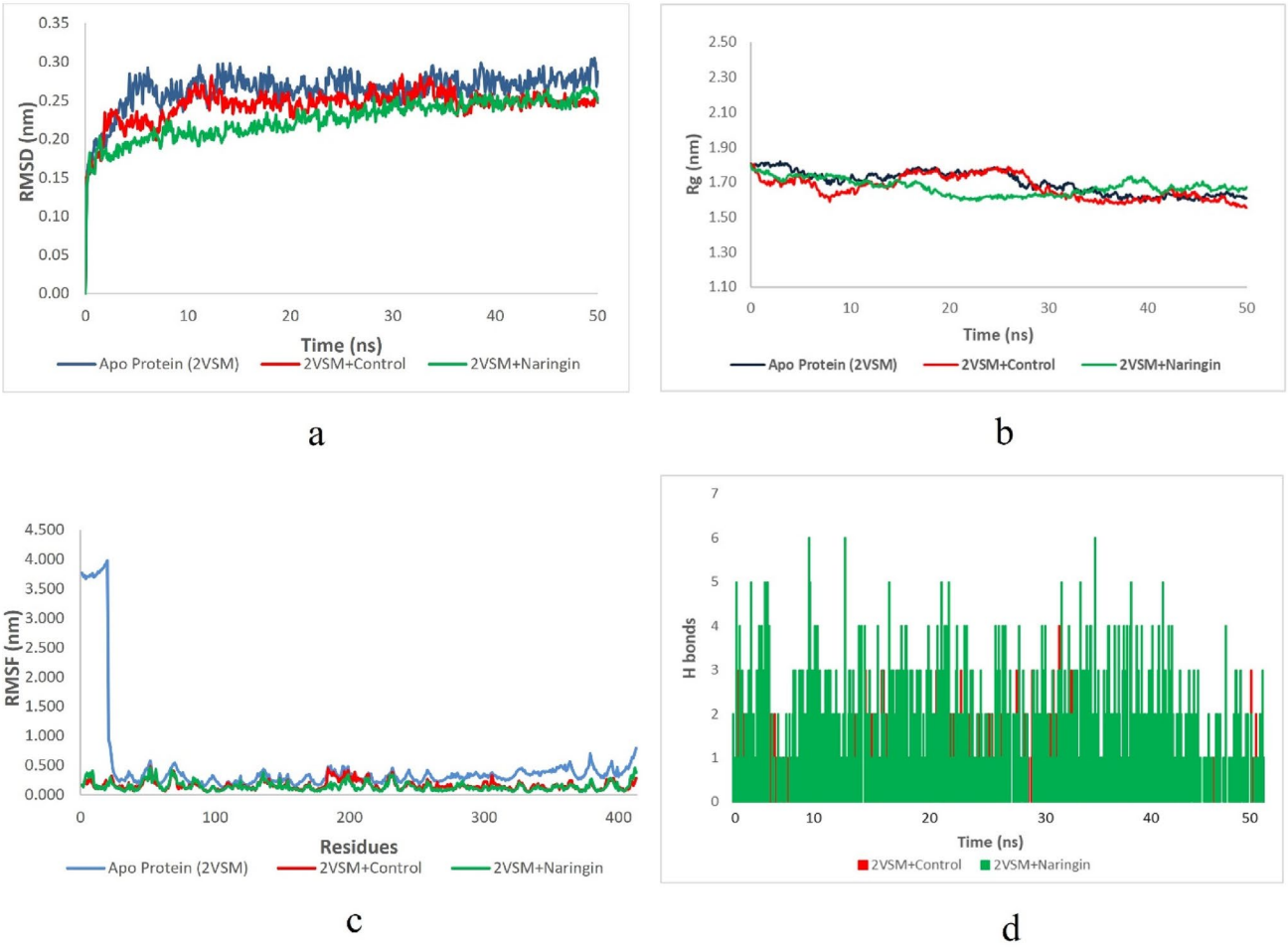


**Fig. 6** Molecular dynamic (MD) simulations of apo protein Nipah Virus Attachment Glycoprotein (PDB id 2VSM), 2VSM-Ribavirin complex, 2VSM-Naringin complex: **a** Root-Mean-Square Deviation (RMSD), **b** Radius of Gyration, **c** Root-Mean-Square Fluctuation (RMSF) and **d** Ligand–Protein H bonds

**Table 7** MM-PBSA calculations of binding free energy for protein–ligand complexes

| Types of binding energy | Binding energy Naringin-NiVG complex | Binding energy Ribavirin-NiVG complex |
|---|---|---|
| ΔG_Binding (kJ $mol^{-1}$) | −218.664 | −83.812 |
| ΔG_Non Polar (kJ $mol^{-1}$) | −20.776 | −10.191 |
| ΔG_Polar (kJ $mol^{-1}$) | 98.736 | 41.474 |
| ΔG_Electrostatic (kJ $mol^{-1}$) | −25.587 | −9.041 |
| ΔG_van der Waals (kJ $mol^{-1}$) | −271.038 | −106.053 |

of the ligand with the target protein. The free energy can be estimated by using the advanced methodology of MM-PBSA. This method, associated with a high computational cost, generates significantly more accurate results than the conventional score-based molecular docking technique (Ren et al. 2015; Singh et al. 2022; Singh and Purohit 2023). Idris et al. (2021) performed MM-PBSA analysis and showed that two ZINC compounds ZINC64606047 and ZINC05296775 could strongly bind with Transmembrane serine protease 2. van der Waals with the binding energies $-190.75 \pm 16.39$ and $-140.16 \pm 14.93$ kJ $mol^{-1}$ respectively. Similarly, Elkarhat et al. (2022) reported high values like $-191.982$ kJ $mol^{-1}$ for SARS-CoV-2 nsp12–streptolydigin and $-153.583$ kJ $mol^{-1}$ for nsp12-VXR complexes, respectively in, 30 ns MD simulation MM-PBSA analysis. Electrostatic, Non-Polar and Polar interaction parameters were associated with the dynamic stability of a protein–ligand complex. A low contribution in binding was shown by unfavourable polar solvation energy (He et al. 2014). In this study, van der Waals contributed more negative energy than its Electrostatic

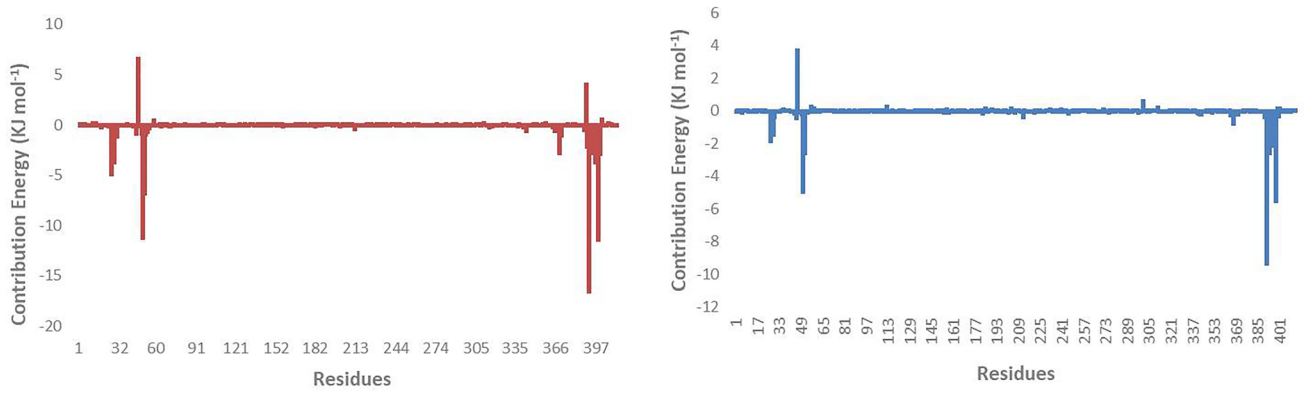


**Fig. 7** Contribution energy plots of interacting amino acids of target proteins (Nipah virus attachment glycoprotein) to Naringin and the control drug, Ribavirin

**Table 8** Amino acid residues of target protein NiV:G and ligand complexes, with at least one hydrogen bond formed during MD simulation

| Naringin | | Ribavirin | |
|---|---|---|---|
| Residues | Contribution energy (kJ $mol^{-1}$) | Residues | Contribution energy (kJ $mol^{-1}$) |
| THR-25 | −0.1337 | CYS50 | −4.9453 |
| CYS26 | −4.9108 | SER51 | −2.5772 |
| THR28 | −3.7219 | TYR391 | −9.3564 |
| SER51 | −6.8337 | THR393 | −2.5875 |
| GLN369 | −2.8437 | ASN396 | −2.1573 |
| ILE390 | −2.2079 | ILE398 | −5.5287 |
| THR393 | −2.8026 | | |
| ASN396 | −3.7571 | | |
| ILE398 | −11.497 | | |
| PRO400 | −2.949 | | |

counterpart (Table 7). The residues, namely THR25, CYS26, THR28, SER51, GLN369, ILE390, THR393, ASN396, ILE398, and PRO400 had the major contributions in the binding of Naringin towards the NiV G protein Fig. 7. Important residues for Ribavirin- NiV G protein, were noted as CYS50, SER51, TYR391, THR393, ASN396 and ILE398 (Table 7 and Fig. 7). The hydrogen bonds along with the contribution energies of these residues are listed in Table 8.

## Structural changes in the native Nipah Virus attachment glycoprotein after binding of control drug and ligand

The distances between randomly flagged amino acids were measured to understand the structural impact on Nipah Virus Attachment Glycoprotein (apo) upon binding with the ligand, Naringin and the control drug, Ribavirin (Fig. 8). A steady decrease in the distances of amino acids in the ligand–protein complex, in comparison with the apo protein (ligand-free) indicated that the alteration of the size of the active site might lead to loss of the enzymatic activity of the target protein NiV G:A (Table 9).

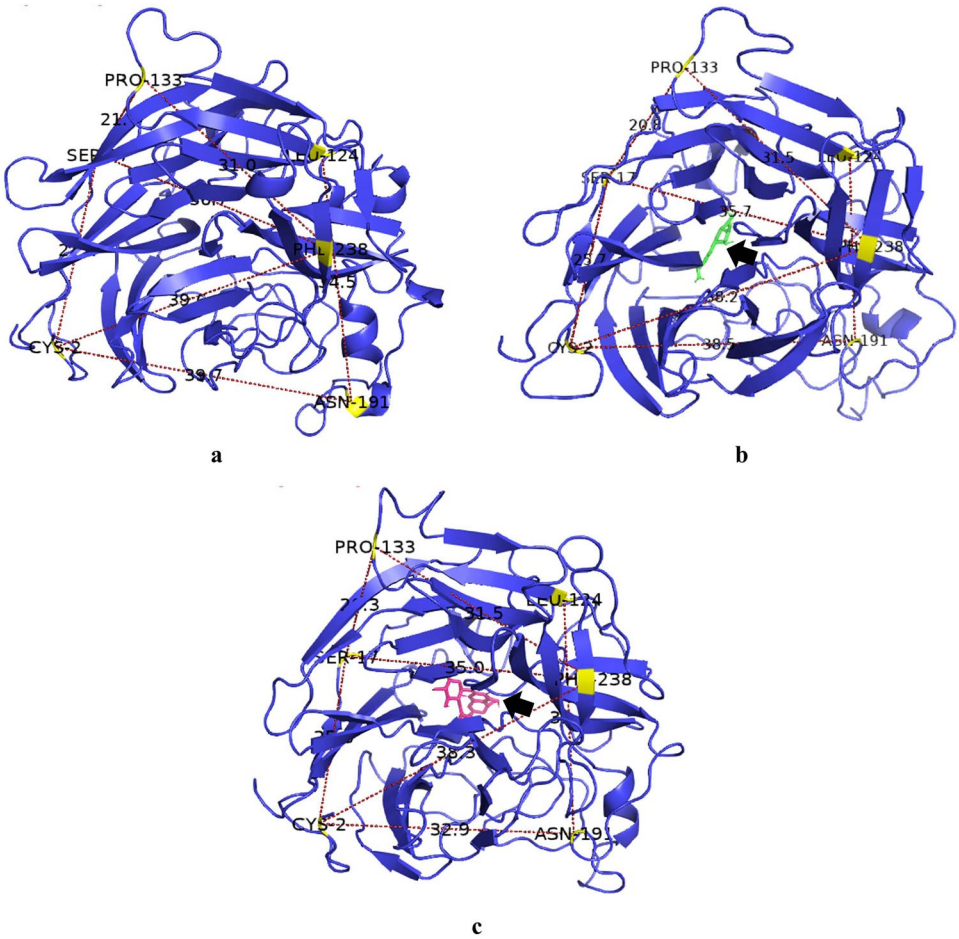


**Fig. 8** Structural comparison by PyMol 2.0 software for **a** Nipah virus attachment glycoprotein chain A (NiV G:A) (Apo); **b** control drug, Ribavirin + NiV G:A and **c** Naringin + NiV G:A

**Table 9** Distance analysis between flagged amino acids of ligand free protein and selected complexes

| Complex | Bond length (Å) | | | | | | |
|---|---|---|---|---|---|---|---|
| | CYS2-SER17 | CYS2-PHE238 | CYS2-ASN191 | LEU124-ASN191 | SER17-PHE238 | SER17-PRO133 | PRO133-PHE238 |
| NiV G:A (Apo) | 27.2 | 39.6 | 39.7 | 34.5 | 36.7 | 21.8 | 31.0 |
| NiV G:A + Ribavirin | 25.7 | 38.2 | 38.5 | 25.5 | 35.7 | 20.8 | 31.5 |
| NiV G:A + Naringin | 25.8 | 38.3 | 32.9 | 31.0 | 35.0 | 20.3 | 31.5 |

**NiV G:A:** Nipah Virus attachment glycoprotein (Chain A)

## Conclusion

Naringin, among the fifty-three screened phytochemicals, showed the most potent inhibitory potential with the Nipah virus glycoprotein (NiV G) (−9.19 kcal $mol^{-1}$) when compared with the control drug, Ribavirin (−6.95 kcal $mol^{-1}$). Other three phytochemicals, Mulberrofuran B, Rutin and Quercetin 3-galactoside, were also found to have strong binding affinities for the target protein. The pharmacophores, four H bond acceptors, one H bond donor and two aromatic groups were found to be responsible for effective protein–ligand interaction. Finally, as revealed by MD simulation, Naringin could form a stable complex with the target protein, NiV G, in the near-native physiological environment.

**Supplementary Information** The online version contains supplementary material available at https://doi.org/10.1007/s13205-023-03595-y.

**Acknowledgements** The authors acknowledge the Centre for Academic and Professional support for correcting and editing the manuscript as per professional English language requirement.

**Data availability** All data supporting the findings of this study are available within the paper and its Supplementary Information. Additional data may be available on request.

## Declarations

**Conflict of interest** The authors declare there is no conflict of interest.

## References


Adel A, Elnaggar MS, Albohy A et al (2022) Evaluation of antiviral activity of *Carica papaya* leaves against SARS-CoV-2 assisted by metabolomic profiling. RSC Adv 12:32844–32852. https://doi.org/10.1039/D2RA04600H

Aguilar-Guadarrama A, Rios M (2018) Flavonoids, sterols and lignans from cochlospermum vitifolium and their relationship with its liver activity. Molecules 23:1952. https://doi.org/10.3390/molecules23081952

Ahmad SB (2014) Nipah Encephalitis – An Update. 69:9

Alamri MA, Altharawi A, Alabbas AB et al (2020) Structure-based virtual screening and molecular dynamics of phytochemicals derived from Saudi medicinal plants to identify potential COVID-19 therapeutics. Arab J Chem 13:7224–7234. https://doi.org/10.1016/j.arabjc.2020.08.004

Aljofan M, Saubern S, Meyer AG et al (2009) Characteristics of Nipah virus and Hendra virus replication in different cell lines and their suitability for antiviral screening. Virus Res 142:92–99. https://doi.org/10.1016/j.virusres.2009.01.014

Amin Huseen NH (2020) Docking study of naringin binding with COVID-19 main protease enzyme. Iraqi J Pharm Sci P-ISSN 1683 - 3597 E-ISSN 2521 - 3512 29:231–238. https://doi.org/10.31351/vol29iss2pp231-238

Ang BSP, Lim TCC, Wang L (2018) Nipah Virus Infection. J Clin Microbiol. https://doi.org/10.1128/JCM.01875-17

Basu S, Veeraraghavan B, Ramaiah S, Anbarasu A (2020) Novel cyclohexanone compound as a potential ligand against SARS-CoV-2 main-protease. Microb Pathog 149:104546. https://doi.org/10.1016/j.micpath.2020.104546

Ben-Shabat S, Yarmolinsky L, Porat D, Dahan A (2020) Antiviral effect of phytochemicals from medicinal plants: Applications and drug delivery strategies. Drug Deliv Transl Res 10:354–367. https://doi.org/10.1007/s13346-019-00691-6

Berman HM, Battistuz T, Bhat TN et al (2002) The protein data bank. Acta Crystallogr D Biol Crystallogr 58:899–907. https://doi.org/10.1107/S0907444902003451

Bhattacharya M, Sharma AR, Patra P et al (2020) A SARS-CoV-2 vaccine candidate: In-silico cloning and validation. Inform Med Unlocked 20:100394. https://doi.org/10.1016/j.imu.2020.100394

Bhowmik D, Nandi R, Jagadeesan R et al (2020) Identification of potential inhibitors against SARS-CoV-2 by targeting proteins responsible for envelope formation and virion assembly using docking based virtual screening, and pharmacokinetics approaches. Infect Genet Evol 84:104451. https://doi.org/10.1016/j.meegid.2020.104451

Byler KG, Ogungbe IV, Setzer WN (2016) In-silico screening for anti-Zika virus phytochemicals. J Mol Graph Model 69:78–91. https://doi.org/10.1016/j.jmgm.2016.08.011

Cataneo AHD, Kuczera D, Koishi AC et al (2019) The citrus flavonoid naringenin impairs the in vitro infection of human cells by Zika virus. Sci Rep 9:16348. https://doi.org/10.1038/s41598-019-52626-3

Chakravarthy DS (2021) Homoeopathic management of polycystic ovarian disease & cholelithiasis with Chionanthus virginicus: A case report. Int J Homoeopath Sci 5:25–29. https://doi.org/10.33545/26164485.2021.v5.i2a.360

Chattu V, Kumar R, Kumary S et al (2018) Nipah virus epidemic in southern India and emphasizing "One Health" approach to ensure global health security. J Fam Med Prim Care 7:275. https://doi.org/10.4103/jfmpc.jfmpc_137_18

Chen Y, Li Z, Pan P et al (2021) Cinnamic acid inhibits Zika virus by inhibiting RdRp activity. Antiviral Res 192:105117. https://doi.org/10.1016/j.antiviral.2021.105117

Chen P, Yang Z, Mai Z et al (2022) Electrospun nanofibrous membrane with antibacterial and antiviral properties decorated with Myoporum bontioides extract and silver-doped carbon nitride nanoparticles for medical masks application. Sep Purif Technol 298:121565. https://doi.org/10.1016/j.seppur.2022.121565

Chiang L-C, Ng L-T, Cheng P-W et al (2005) Antiviral activities of extracts and selected pure constituents of Ocimum basilicum. Clin Exp Pharmacol Physiol 32:811–816. https://doi.org/10.1111/j.1440-1681.2005.04270.x

Cho C, Li SG, Lalonde TJ et al (2022) Drug Repurposing for the SARS-CoV-2 Papain-Like Protease. ChemMedChem. https://doi.org/10.1002/cmdc.202100455

Choi HG, Lee HD, Kim SH et al (2013) Phenolic Glycosides from *Lindera obtusiloba* and their Anti-allergic Inflammatory Activities. Nat Prod Commun. https://doi.org/10.1177/1934578X1300800212

Chong H-T, Kamarulzaman A, Tan C-T et al (2001) Treatment of acute Nipah encephalitis with ribavirin. Ann Neurol 49:810–813. https://doi.org/10.1002/ana.1062

Chou S-C, Huang T-J, Lin E-H et al (2012) Antihepatitis B Virus Constituents of *Solanum Erianthum*. Nat Prod Commun. https://doi.org/10.1177/1934578X1200700205

Chua KB, Bellini WJ, Rota PA et al (2000) Nipah Virus: a recently emergent deadly paramyxovirus. Science 288:1432–1435. https://doi.org/10.1126/science.288.5470.1432

Chua KB, Lek Koh C, Hooi PS et al (2002) Isolation of Nipah virus from Malaysian Island flying-foxes. Microbes Infect 4:145–151. https://doi.org/10.1016/S1286-4579(01)01522-2

Colunga Biancatelli RML, Berrill M, Catravas JD, Marik PE (2020) Quercetin and Vitamin C: an experimental, synergistic therapy for the prevention and treatment of SARS-CoV-2 related disease (COVID-19). Front Immunol 11:1451. https://doi.org/10.3389/fimmu.2020.01451

Constantinides PP, Wasan KM (2007) Lipid formulation strategies for enhancing intestinal transport and absorption of P-glycoprotein (P-gp) substrate drugs: in vitro/in vivo case studies. J Pharm Sci 96:235–248. https://doi.org/10.1002/jps.20780

da Cruz Freire JE, Júnior JEM, Pinheiro DP et al (2022) Evaluation of the anti-diabetic drug sitagliptin as a novel attenuate to SARS-CoV-2 evidence-based in silico: molecular docking and molecular dynamics. 3 Biotech 12:344. https://doi.org/10.1007/s13205-022-03406-w

Daina A, Michielin O, Zoete V (2017) SwissADME: a free web tool to evaluate pharmacokinetics, drug-likeness and medicinal chemistry friendliness of small molecules. Sci Rep 7:42717. https://doi.org/10.1038/srep42717

de Wit E, Munster VJ (2015) Animal models of disease shed light on Nipah virus pathogenesis and transmission: Nipah virus pathogenesis and transmission. J Pathol 235:196–205. https://doi.org/10.1002/path.4444

Devnath P, Masud HMAA (2021) Nipah virus: a potential pandemic agent in the context of the current severe acute respiratory syndrome coronavirus 2 pandemic. New Microbes New Infect 41:100873. https://doi.org/10.1016/j.nmni.2021.100873

Dhiman A (2022) Purohit R (2022) Identification of potential mutational hotspots in serratiopeptidase to address its poor pH tolerance issue. J Biomol Struct Dyn. https://doi.org/10.1080/07391102.2022.2137699

Doak BC, Over B, Giordanetto F, Kihlberg J (2014) Oral druggable space beyond the rule of 5: insights from drugs and clinical candidates. Chem Biol 21:1115–1142. https://doi.org/10.1016/j.chembiol.2014.08.013

Dong J, Wang N-N, Yao Z-J et al (2018) ADMETlab: a platform for systematic ADMET evaluation based on a comprehensively collected ADMET database. J Cheminformatics 10:29. https://doi.org/10.1186/s13321-018-0283-x

Elkarhat Z, Charoute H, Elkhattabi L et al (2022) Potential inhibitors of SARS-cov-2 RNA dependent RNA polymerase protein: molecular docking, molecular dynamics simulations and MM-PBSA analyses. J Biomol Struct Dyn 40:361–374. https://doi.org/10.1080/07391102.2020.1813628

Erdemli H, Akyol S, Armutcu F, Akyol O (2015) Antiviral properties of caffeic acid phenethyl ester and its potential application. J Intercult Ethnopharmacol 4:344. https://doi.org/10.5455/jice.20151012013034

Ertl P, Rohde B, Selzer P (2000) Fast calculation of molecular polar surface area as a sum of fragment-based contributions and its application to the prediction of drug transport properties. J Med Chem 43:3714–3717. https://doi.org/10.1021/jm000942e

Fatima K, Mathew S, Suhail M et al (2014) Docking studies of Pakistani HCV NS3 Helicase: a possible antiviral drug target. PLoS ONE 9:e106339. https://doi.org/10.1371/journal.pone.0106339

Fatriansyah JF, Rizqillah RK, Yandi MY (2022) Molecular docking and molecular dynamics simulation of fisetin, galangin, hesperetin, hesperidin, myricetin, and naringenin against polymerase of Dengue virus. J Trop Med 2022:1–12. https://doi.org/10.1155/2022/7254990

Gaieb Z, Parks CD, Chiu M et al (2019) D3R grand challenge 3: blind prediction of protein–ligand poses and affinity rankings. J Comput Aided Mol Des 33:1–18. https://doi.org/10.1007/s10822-018-0180-4

Geiger N, König E-M, Oberwinkler H et al (2022) Acetylsalicylic acid and salicylic acid inhibit SARS-CoV-2 replication in precision-cut lung slices. Vaccines 10:1619. https://doi.org/10.3390/vaccines10101619

Geisbert TW, Bobb K, Borisevich V et al (2021) A single dose investigational subunit vaccine for human use against Nipah virus and Hendra virus. Npj Vaccines 6:23. https://doi.org/10.1038/s41541-021-00284-w

Ghimire S, Shahrear S, Saigaonkar SK, Harris LK (2022) Identification of Potential Inhibitors against Attachment Glycoprotein G of Nipah virus using Comprehensive Drug Repurposing Approach

Glaab E, Manoharan GB, Abankwa D (2021) Pharmacophore model for SARS-CoV-2 3CLpro small-molecule inhibitors and *in Vitro* experimental validation of computationally screened inhibitors. J Chem Inf Model 61:4082–4096. https://doi.org/10.1021/acs.jcim.1c00258

Gupta A, Ahmad R, Siddiqui S et al (2022) Flavonol morin targets host ACE2, IMP-α, PARP-1 and viral proteins of SARS-CoV-2, SARS-CoV and MERS-CoV critical for infection and survival: a computational analysis. J Biomol Struct Dyn 40:5515–5546. https://doi.org/10.1080/07391102.2021.1871863

Gurley ES, Montgomery JM, Hossain MJ et al (2007) Person-to-person transmission of Nipah virus in a Bangladeshi community. Emerg Infect Dis 13:1031–1037. https://doi.org/10.3201/eid1307.061128

Hanwell MD, Curtis DE, Lonie DC et al (2012) Avogadro: an advanced semantic chemical editor, visualization, and analysis platform. J Cheminform 4:17. https://doi.org/10.1186/1758-2946-4-17

Hasan AH, Hussen NH, Shakya S et al (2022) In silico discovery of multi-targeting inhibitors for the COVID-19 treatment by molecular docking, molecular dynamics simulation studies, and ADMET predictions. Struct Chem 33:1645–1665. https://doi.org/10.1007/s11224-022-01996-y

Hauser N, Gushiken AC, Narayanan S et al (2021) Evolution of Nipah virus infection: past, present, and future considerations. Trop Med Infect Dis 6:24. https://doi.org/10.3390/tropicalmed6010024

He J-Y, Li C, Wu G (2014) Discovery of potential drugs for human-infecting H7N9 virus containing R294K mutation. Drug Des Devel Ther. https://doi.org/10.2147/DDDT.S74061

Hou T, Wang J (2008) Structure – ADME relationship: still a long way to go? Expert Opin Drug Metab Toxicol 4:759–770. https://doi.org/10.1517/17425255.4.6.759

Hu B, Guo H, Zhou P, Shi Z-L (2021) Characteristics of SARS-CoV-2 and COVID-19. Nat Rev Microbiol 19:141–154. https://doi.org/10.1038/s41579-020-00459-7

Huang J, Rauscher S, Nawrocki G et al (2017) CHARMM36m: an improved force field for folded and intrinsically disordered proteins. Nat Methods 14:71–73. https://doi.org/10.1038/nmeth.4067

Ibrahim AK, Youssef AI, Arafa AS, Ahmed SA (2013) Anti-H5N1 virus flavonoids from *Capparis sinaica* Veill. Nat Prod Res 27:2149–2153. https://doi.org/10.1080/14786419.2013.790027

Ibrahim ZY, Uzairu A, Shallangwa GA, Abechi SE (2021) Pharmacokinetic predictions and docking studies of substituted aryl amine-based triazolopyrimidine designed inhibitors of Plasmodium falciparum dihydroorotate dehydrogenase (PfDHODH). Future J Pharm Sci 7:133. https://doi.org/10.1186/s43094-021-00288-2

Idris MO, Yekeen AA, Alakanse OS, Durojaye OA (2021) Computer-aided screening for potential TMPRSS2 inhibitors: a combination of pharmacophore modeling, molecular docking and molecular dynamics simulation approaches. J Biomol Struct Dyn 39:5638–5656. https://doi.org/10.1080/07391102.2020.1792346

Jamhour RMAQ, Al-Nadaf AH, Wedian F et al (2022) Phytochemicals as a potential inhibitor of COVID-19: an in-silico perspective. Russ J Phys Chem A 96:1589–1597. https://doi.org/10.1134/S0036024422070251

Jesus MD, Gaza JT, Junio H, Nellas R (2020) Associated receptors ACE2, spike protein RBD, and TMPRSS2. 27

Jolliffe IT, Cadima J (2016) Principal component analysis: a review and recent developments. Philos Trans R Soc Math Phys Eng Sci 374:20150202. https://doi.org/10.1098/rsta.2015.0202

Kalbhor MS, Bhowmick S, Alanazi AM et al (2021) Multi-step molecular docking and dynamics simulation-based screening of large antiviral specific chemical libraries for identification of Nipah virus glycoprotein inhibitors. Biophys Chem 270:106537. https://doi.org/10.1016/j.bpc.2020.106537

Karpiński TM, Kwaśniewski M, Ożarowski M, Alam R (2021) *In silico* studies of selected xanthophylls as potential candidates against SARS-CoV-2 targeting main protease (Mpro) and papain-like protease (PLpro). Herba Pol 67:1–8. https://doi.org/10.2478/hepo-2021-0009

Keflie TS, Biesalski HK (2021) Micronutrients and bioactive substances: Their potential roles in combating COVID-19. Nutrition 84:111103. https://doi.org/10.1016/j.nut.2020.111103

Keretsu S, Bhujbal SP, Cho SJ (2020) Rational approach toward COVID-19 main protease inhibitors via molecular docking, molecular dynamics simulation and free energy calculation. Sci Rep 10:17716. https://doi.org/10.1038/s41598-020-74468-0

Khan SL, Siddiqui FA (2020) Beta-Sitosterol: as immunostimulant, antioxidant and inhibitor of SARS-CoV-2 spike glycoprotein. Arch Pharmacol Ther 2:12–16. https://doi.org/10.33696/Pharmacol.2.014

Khazdair M, Anaeigoudari A, Agbor G (2021) Anti-viral and anti-inflammatory effects of kaempferol and quercetin and COVID-2019: A scoping review. Asian Pac J Trop Biomed 11:327. https://doi.org/10.4103/2221-1691.319567

Kim S, Chen J, Cheng T et al (2019) PubChem 2019 update: improved access to chemical data. Nucleic Acids Res 47:D1102–D1109. https://doi.org/10.1093/nar/gky1033

Kozakov D, Hall DR, Xia B et al (2017) The ClusPro web server for protein–protein docking. Nat Protoc 12:255–278. https://doi.org/10.1038/nprot.2016.169

Kumar S, Bhardwaj VK, Singh R, Purohit R (2023) Structure restoration and aggregate inhibition of V30M mutant transthyretin protein by potential quinoline molecules. Int J Biol Macromol 231:123318. https://doi.org/10.1016/j.ijbiomac.2023.123318

Kumari R, Kumar R, Open Source Drug Discovery Consortium, Lynn A (2014) *g_mmpbsa* —A GROMACS Tool for High-Throughput MM-PBSA Calculations. J Chem Inf Model 54:1951–1962. https://doi.org/10.1021/ci500020m

Kumari M, Singh R, Subbarao N (2021) Exploring the interaction mechanism between potential inhibitor and multi-target Mur enzymes of mycobacterium tuberculosis using molecular docking, molecular dynamics simulation, principal component analysis, free energy landscape, dynamic cross-correlation matrices, vector movements, and binding free energy calculation. J Biomol Struct Dyn https://doi.org/10.1080/07391102.2021.1989040

Kushwaha PP, Singh AK, Bansal T et al (2021) Identification of natural inhibitors against SARS-CoV-2 drugable targets using molecular docking, molecular dynamics simulation, and MM-PBSA approach. Front Cell Infect Microbiol 11:730288. https://doi.org/10.3389/fcimb.2021.730288

Laskowski RA (2009) PDBsum new things. Nucleic Acids Res 37:D355–D359. https://doi.org/10.1093/nar/gkn860

Le QU, Joshi RK, Lay HL, Chang M (2018) Agrimonia pilosa Ledeb: Phytochemistry, Ethnopharmacology, Pharmacology of an important traditional herbal medicine

Lever J, Krzywinski M, Altman N (2017) Principal component analysis. Nat Methods 14:641–642. https://doi.org/10.1038/nmeth.4346

Li J-X, Shi Q, Xiong Q-B et al (1998) Tribulusamide A and B, new hepatoprotective lignanamides from the fruits of *Tribulus terrestris* : indications of Cytoprotective activity in murine hepatocyte culture. Planta Med 64:628–631. https://doi.org/10.1055/s-2006-957535

Li J, Meng A-P, Guan X-L et al (2013) Anti-hepatitis B virus lignans from the root of Streblus asper. Bioorg Med Chem Lett 23:2238–2244. https://doi.org/10.1016/j.bmcl.2013.01.046

Lima CS, Mottin M, de Assis LR et al (2021) Flavonoids from Pterogyne nitens as Zika virus NS2B-NS3 protease inhibitors. Bioorganic Chem 109:104719. https://doi.org/10.1016/j.bioorg.2021.104719

Lipinski CA, Lombardo F, Dominy BW, Feeney PJ (2001) Experimental and computational approaches to estimate solubility and permeability in drug discovery and development settingsq. Adv Drug Deliv Rev

Liu W, Zheng W, Cheng L et al (2022) Citrus fruits are rich in flavonoids for immunoregulation and potential targeting ACE2. Nat Prod Bioprospecting 12:4. https://doi.org/10.1007/s13659-022-00325-4

Luo H-J, Wang J-Z, Chen J-F, Zou K (2011) Docking study on chlorogenic acid as a potential H5N1 influenza A virus neuraminidase inhibitor. Med Chem Res 20:554–557. https://doi.org/10.1007/s00044-010-9336-z

Makhloufi A, Ghemit R, Kolli M el (2022) Spike Protein Potential Receptors Study: Comparative Computational Analysis Approach on SARS-CoV-2 -AC2/CD147 Complexes. Biointerface Res Appl Chem 13:351. https://doi.org/10.33263/BRIAC134.351

Martinez-Gil L, Vera-Velasco NM, Mingarro I (2017) Exploring the human-Nipah virus protein-protein interactome. J Virol. https://doi.org/10.1128/JVI.01461-17

Martins B de A, Sande D, Solares MD, Takahashi JA (2021) Antioxidant role of morusin and mulberrofuran B in ethanol extract of *Morus alba* roots. Nat Prod Res 35:5993–5996. https://doi.org/10.1080/14786419.2020.1810036

Mehand MS, Al-Shorbaji F, Millett P, Murgue B (2018) The WHO R&D Blueprint: 2018 review of emerging infectious diseases requiring urgent research and development efforts. Antiviral Res 159:63–67. https://doi.org/10.1016/j.antiviral.2018.09.009

Miserocchi E, Modorati G, Galli L, Rama P (2007) Efficacy of valacyclovir vs acyclovir for the prevention of recurrent herpes simplex virus eye disease: a pilot study. Am J Ophthalmol 144:547-551.e1. https://doi.org/10.1016/j.ajo.2007.06.001

Mohammed IA (2021) Virtual screening of Microalgal compounds as potential inhibitors of Type 2 Human Transmembrane serine protease (TMPRSS2). 25

Mou J, Lin X, Su H et al (2021) Anti-hepatitis B virus activity and hepatoprotective effect of des(rhamnosyl) verbascoside from *Lindernia ruellioides* in vitro. Phytother Res 35:4555–4566. https://doi.org/10.1002/ptr.7159

Nag A, Banerjee R (2021) Network pharmacological evaluation for identifying novel drug-like molecules from ginger (Zingiber officinale Rosc.) against multiple disease targets, a computational biotechnology approach. Netw Model Anal Health Inform Bioinforma 10:55. https://doi.org/10.1007/s13721-021-00330-6

Nag A, Banerjee R, Chowdhury RR, Krishnapura Venkatesh C (2021a) Phytochemicals as potential drug candidates for targeting SARS CoV 2 proteins, an in silico study. VirusDisease 32:98–107. https://doi.org/10.1007/s13337-021-00654-x

Nag A, Paul S, Banerjee R, Kundu R (2021b) In silico study of some selective phytochemicals against a hypothetical SARS-CoV-2 spike RBD using molecular docking tools. Comput Biol Med 137:104818. https://doi.org/10.1016/j.compbiomed.2021.104818

Nag A, Banerjee R, Paul S, Kundu R (2022) Curcumin inhibits spike protein of new SARS-CoV-2 variant of concern (VOC) Omicron, an in silico study. Comput Biol Med 146:105552. https://doi.org/10.1016/j.compbiomed.2022.105552

Nag A, Dhull N, Gupta A (2022) Evaluation of tea (Camellia sinensis L.) phytochemicals as multi-disease modulators, a multidimensional in silico strategy with the combinations of network pharmacology, pharmacophore analysis, statistics and molecular docking. Mol Divers. https://doi.org/10.1007/s11030-022-10437-1

Nag A, Dasgupta A, Sengupta S et al (2023) An in-silico pharmacophore-based molecular docking study to evaluate the inhibitory potentials of novel fungal triterpenoid Astrakurkurone analogues against a hypothetical mutated main protease of SARS-CoV-2 virus. Comput Biol Med 152:106433. https://doi.org/10.1016/j.compbiomed.2022.106433

Nandagoapalan V, Doss A, Marimuthu C (2016) Phytochemical Analysis of Some Traditional Medicinal Plants. 5

Ong KC, Khoo H-E (1997) Biological effects of myricetin. Gen Pharmacol Vasc Syst 29:121–126. https://doi.org/10.1016/S0306-3623(96)00421-1

Orfali R, Rateb ME, Hassan HM et al (2021) Sinapic acid suppresses SARS CoV-2 replication by targeting its envelope protein. Antibiotics 10:420. https://doi.org/10.3390/antibiotics10040420

Pandey P, Rane JS, Chatterjee A et al (2021) Targeting SARS-CoV-2 spike protein of COVID-19 with naturally occurring phytochemicals: an *in silico* study for drug development. J Biomol Struct Dyn 39:6306–6316. https://doi.org/10.1080/07391102.2020.1796811

Pang R, Tao J-Y, Zhang S-L et al (2010) In vitro antiviral activity of lutein against hepatitis B virus. Phytother Res 24:1627–1630. https://doi.org/10.1002/ptr.3155

Parang K, Wiebe LI, Knaus EE et al (1997) In vitro antiviral activities of myristic acid analogs against human immunodeficiency and

hepatitis B viruses. Antiviral Res 34:75–90. https://doi.org/10.1016/S0166-3542(96)01022-4
Paton NI, Leo YS, Zaki SR et al (1999) Outbreak of Nipah-virus infection among abattoir workers in Singapore. The Lancet 354:1253–1256. https://doi.org/10.1016/S0140-6736(99)04379-2
Pawar KS, Mastud RN, Pawar SK et al (2021) Oral curcumin with piperine as adjuvant therapy for the treatment of COVID-19: a randomized clinical trial. Front Pharmacol 12:669362. https://doi.org/10.3389/fphar.2021.669362
Pei K, Ou J, Huang J, Ou S (2016) *p* -Coumaric acid and its conjugates: dietary sources, pharmacokinetic properties and biological activities: *p* -Coumaric acid and its conjugates. J Sci Food Agric 96:2952–2962. https://doi.org/10.1002/jsfa.7578
Pettersen EF, Goddard TD, Huang CC et al (2004) UCSF Chimera?A visualization system for exploratory research and analysis. J Comput Chem 25:1605–1612. https://doi.org/10.1002/jcc.20084
Pournaghi N, Khalighi-Sigaroodi F, Safari E, Hajiaghaee R (2020) A review of the genus Caesalpinia L.: emphasis on the cassane and norcassane compounds and cytotoxicity effects. J Med Plants 19:1–20. https://doi.org/10.29252/jmp.19.76.1
Priyadarsinee L, Sarma H, Sastry GN (2022) Glycoprotein attachment with host cell surface receptor ephrin B2 and B3 in mediating entry of nipah and hendra virus: a computational investigation. J Chem Sci 134:114. https://doi.org/10.1007/s12039-022-02110-9
Qazi S, Das S, Khuntia BK et al (2021) In Silico molecular docking and molecular dynamic simulation analysis of phytochemicals from Indian foods as potential inhibitors of SARS-CoV-2 RdRp and 3CLpro. Nat Prod Commun. https://doi.org/10.1177/1934578X211031707
Radhakrishnan N, Lam KW, Esa NM (2017) Molecular docking analysis of Carica papaya Linn constituents as antiviral agent. Mol Docking Anal Carica Papaya Linn Const Antivir Agent
Randhawa V, Pathania S, Kumar M (2022) Computational identification of potential multitarget inhibitors of Nipah virus by molecular docking and molecular dynamics. Microorganisms 10:1181. https://doi.org/10.3390/microorganisms10061181
Rao P, Shukla A, Parmar P et al (2020) Reckoning a fungal metabolite, Pyranonigrin A as a potential Main protease (Mpro) inhibitor of novel SARS-CoV-2 virus identified using docking and molecular dynamics simulation. Biophys Chem 264:106425. https://doi.org/10.1016/j.bpc.2020.106425
Ren W, Truong TM, Ai H (2015) Study of the binding energies between unnatural amino acids and engineered orthogonal tyrosyl-tRNA synthetases. Sci Rep 5:12632. https://doi.org/10.1038/srep12632
Ropón-Palacios G, Chenet-Zuta ME, Olivos-Ramirez GE et al (2020) Potential novel inhibitors against emerging zoonotic pathogen *Nipah virus* : a virtual screening and molecular dynamics approach. J Biomol Struct Dyn 38:3225–3234. https://doi.org/10.1080/07391102.2019.1655480
Sales-Campos H, Reis de Souza P, Crema Peghini B et al (2013) An overview of the modulatory effects of oleic acid in health and disease. Mini-Rev Med Chem 13:201–210. https://doi.org/10.2174/1389557511313020003
Santos KB, Guedes IA, Karl ALM, Dardenne LE (2020) Highly flexible ligand docking: benchmarking of the DockThor program on the LEADS-PEP protein-peptide data set. J Chem Inf Model 60:667–683. https://doi.org/10.1021/acs.jcim.9b00905
Schneidman-Duhovny D, Dror O, Inbar Y et al (2008) PharmaGist: a webserver for ligand-based pharmacophore detection. Nucleic Acids Res 36:W223–W228. https://doi.org/10.1093/nar/gkn187
Schüttelkopf AW, van Aalten DMF (2004) *PRODRG* : a tool for high-throughput crystallography of protein–ligand complexes. Acta Crystallogr D Biol Crystallogr 60:1355–1363. https://doi.org/10.1107/S0907444904011679
Seeliger D, de Groot BL (2010) Ligand docking and binding site analysis with PyMOL and Autodock/Vina. J Comput Aided Mol Des 24:417–422. https://doi.org/10.1007/s10822-010-9352-6
Shahhamzehei N, Abdelfatah S, Efferth T (2022) In Silico and in vitro identification of pan-coronaviral main protease inhibitors from a large natural product library. Pharmaceuticals 15:308. https://doi.org/10.3390/ph15030308
Sharma N, Samarakoon K, Gyawali R et al (2014) Evaluation of the antioxidant, anti-inflammatory, and anticancer activities of euphorbia hirta ethanolic extract. Molecules 19:14567–14581. https://doi.org/10.3390/molecules190914567
Sharma V, Kaushik S, Kumar R et al (2019) Emerging trends of Nipah virus: a review. Rev Med Virol 29:e2010. https://doi.org/10.1002/rmv.2010
Sharma N, Tiwari N, Vyas M, et al (2020) An overview of therapeutic effects of vanillic acid
Shukla R, Singh S, Singh A, Misra K (2021) Two pronged approach for prevention and therapy of COVID-19 (Sars-CoV-2) by a multi-targeted herbal drug, a component of ayurvedic decoction. Eur J Integr Med 43:101268. https://doi.org/10.1016/j.eujim.2020.101268
Singh R, Purohit R (2023) Computational analysis of protein-ligand interaction by targeting a cell cycle restrainer. Comput Methods Programs Biomed 231:107367. https://doi.org/10.1016/j.cmpb.2023.107367
Singh R, Bhardwaj VK, Purohit R (2022) Inhibition of nonstructural protein 15 of SARS-CoV-2 by golden spice: A computational insight. Cell Biochem Funct 40:926–934. https://doi.org/10.1002/cbf.3753
Soekamto NH, Firdaus Ahmad F, Appa FE (2019) Potential of stigmasterol from EtOAc extract Melochia umbellata (Houtt) Stapf var. Visenia as Dengue Antivirus. J Phys Conf Ser 1341:032044. https://doi.org/10.1088/1742-6596/1341/3/032044
Tadayon M, Garkani-Nejad Z (2019) In silico study combining QSAR, docking and molecular dynamics simulation on 2,4-disubstituted pyridopyrimidine derivatives. J Recept Signal Transduct 39:167–174. https://doi.org/10.1080/10799893.2019.1641821
Tang W, Li M, Liu Y et al (2019) Small molecule inhibits respiratory syncytial virus entry and infection by blocking the interaction of the viral fusion protein with the cell membrane. FASEB J 33:4287–4299. https://doi.org/10.1096/fj.201800579R
Thakur V, Thakur P, Ratho RK (2022) Nipah Outbreak: Is it the beginning of another pandemic in the era of COVID-19 and Zika. Brain Behav Immun 99:25–26. https://doi.org/10.1016/j.bbi.2021.09.015
Tigabu B, Rasmussen L, White EL et al (2014) A BSL-4 high-throughput screen identifies sulfonamide inhibitors of Nipah virus. ASSAY Drug Dev Technol 12:155–161. https://doi.org/10.1089/adt.2013.567
Trott O, Olson AJ (2009) AutoDock Vina: Improving the speed and accuracy of docking with a new scoring function, efficient optimization, and multithreading. J Comput Chem NA-NA. https://doi.org/10.1002/jcc.21334
Vanitha S, Chitra F, Dash M (2019) Public Health Awareness of Nipah Virus. 8
Wallace AE (2001) Thiamine treatment of chronic hepatitis B infection. Am J Gastroenterol 96:864–868
Wang G-F, Shi L-P, Ren Y-D et al (2009) Anti-hepatitis B virus activity of chlorogenic acid, quinic acid and caffeic acid in vivo and in vitro. Antiviral Res 83:186–190. https://doi.org/10.1016/j.antiviral.2009.05.002
Wright PJ, Crameri G, Eaton BT (2005) RNA synthesis during infection by Hendra virus: an examination by quantitative real-time PCR of RNA accumulation, the effect of ribavirin and the attenuation of transcription. Arch Virol 150:521–532. https://doi.org/10.1007/s00705-004-0417-5

Xie J, Tan P, Geng F et al (2023) A practical and rapid screening method for influenza virus neuraminidase inhibitors based on fluorescence detection. Anal Sci. https://doi.org/10.1007/s44211-023-00267-y

Xiong G, Wu Z, Yi J et al (2021) ADMETlab 2.0: an integrated online platform for accurate and comprehensive predictions of ADMET properties. Nucleic Acids Res 49:W5–W14. https://doi.org/10.1093/nar/gkab255

Yadav R, Imran M, Dhamija P et al (2021) Virtual screening and dynamics of potential inhibitors targeting RNA binding domain of nucleocapsid phosphoprotein from SARS-CoV-2. J Biomol Struct Dyn 39:4433–4448. https://doi.org/10.1080/07391102.2020.1778536

Yadav P, El-Kafrawy SA, El-Day MM et al (2022) Discovery of small molecules from Echinacea angustifolia targeting RNA-dependent RNA polymerase of Japanese Encephalitis virus. Life 12:952. https://doi.org/10.3390/life12070952